universität
wien

DISSERTATION

Titel der Dissertation

Experimental non-classicality of an indivisible quantum system

Verfasser

Mag. Radosław Łapkiewicz

angestrebter akademischer Grad

Doktor der Naturwissenschaften (Dr. rer. nat.)

Wien, 2012

Studienkennzahl lt. Studienblatt:	A 791 411
Dissertationsgebiet lt. Studienblatt:	Physik, DK: Komplexe Quantensysteme
Betreuerin / Betreuer:	o. Univ.-Prof. Dr. DDr. h. c. Anton Zeilinger

To Maja

“A wooden die can be described only from without. We are therefore condemned to eternal ignorance of its essence. Even if it is quickly cut in two, immediately its inside becomes a wall and there occurs the lightning-swift transformation of a mystery into a skin.

For this reason it is impossible to lay the foundation for the psychology of a stone ball, of an iron bar, or a wooden cube. “

“Wooden Die”, Zbigniew Herbert [1]

Contents

Zusammenfassung

Wie von J. S. Bell gezeigt wurde, können bestimmte quantenmechanische Vorraussagen über Vielteilchensystemen nicht durch Theorien mit lokalen verborgenen Variablen beschrieben werden [2]. Im Experiment wurden jedoch immer die quantenmechanischen Vorhersagen durch mehrere Experimente bestätigt [3, 4, 5]. Bell, Kochen und Specker (BKS) konnten zudem zeigen, dass bereits ein einzelnes quantenmechanisches System nicht mit Hilfe nicht-kontextueller verborgener Variablen korrekt beschrieben werden kann [6, 2, 7]. Basierend auf den Ideen von BKS wurden in letzter Zeit ebenso Ungleichungen entwickelt, die den Unterschied der Quantenmechanik zu einer Theorie mit nicht-kontextuellen verborgenen Variablen deutlich machen [8, 9]. Diese wurden bereits an verschiedenen Systemen, wie z.B. Ionen und Photonen, experimentell getestet [10, 11]. Im Gegensatz zu diesen Experimenten, welche Qubit Paare verwendeten, konnten wir hingegen die Verletzung einer Ungleichung [8] mit einzelnen photonischen Qutrits beobachten. Unserem Wissen nach ist dies die erste experimentelle Falsifizierung von Modellen verbogener Variablen an einem System welches grundsätzlich keine Verschränkung zulässt.

Im ersten Kapitel der hier vorgelegten Arbeit werden die theoretischen Grundlagen sowie deren Ergebnisse präsentiert: das BKS Theorem in seinen verschiedenen Varianten. Zunächst werden die notwendigen Ideen eingeführt, die Hintergründe des Theorems beleuchtet und die mathematische Darstellung formuliert. Anschließend werden die auf dem BKS Theorem beruhenden Experimente besprochen. Zum Schluss wird die von Klyachko, Can, Binicioglu und Shumovsky (KCBS) entwickelte Ungleichung genauer behandelt [8], da diese unserem Experiment zu Grunde liegt.

Im zweiten Kapitel werden die experimentellen Konzepte, welche es uns ermöglichen die KCBS Ungleichung mit einzelnen Photonen zu testen, erläutert [12]. Wir zeigen den Weg von der mathematischen Idee hin zur Physik und dadurch wie mit einem einfachen optischen System die Geometrie des BKS Theorems realisiert werden kann.

Im dritten Kapitel wird der experimentelle Aufbau zur Überprüfung der

KCBS Ungleichung präsentiert. Hierfür wird zum einen auf die experimentelle Erzeugung von Einzelphotonen eingegangen und zum anderen die Entstehung des tatsächlichen Aufbaus ausgehend von mathematischen Konzepten erklärt.

Im vierten Kapitel werden die Methoden zur Datenaufnahme und Auswertung erläutert. Wir konnten ein Wert von -3.893(6) gemessen. Dieser liegt 120 Standardabweichungen unterhalb der klassischen Grenze von -3.081(2) und stell somit eine deutliche Verletzung des klassischen Limits dar. Abschließend werden systematische Effekte diskutiert und auf deren Bedeutung und den Umgang mit ihnen eingegangen.

Abstract

J.S. Bell showed that local hidden variables cannot explain certain quantum mechanical predictions for composite systems [2]. Those predictions have been confirmed by many experiments [3, 4, 5]. Theorems due to Bell, Kochen and Specker (BKS) say that even single quantum systems do not allow descriptions in terms of non-contextual hidden variables [6, 2, 7]. Recently, inequalities, following from the BKS ideas, were derived [8, 9] and some of them were tested experimentally with ions and photons [10, 11]. In contrast to previous experiments in which pairs of qubits were used, we observed a violation of an inequality [8] with single photonic qutrits. To our knowledge, this is the first experiment falsifying hidden variable models with a system which does not allow entanglement.

In the first chapter we present the theoretical notions and results most relevant to our work: the BKS theorem in its various versions. Initially, we introduce the necessary concepts, discuss the background of the theorem, and formulate it. Later, we discuss the experiments rooted in the BKS theorem. Finally, we present the inequality due to Klyachko, Can, Binicioglu and Shumovsky (KCBS) [8].

In the second chapter we describe an experimental scheme allowing us to test this inequality with single photons [12]. We take a step, from mathematics to physics, showing how a simple optical system can realise the geometry of a BKS proof.

The third chapter presents the experimental setup that we used to test the KCBS inequality. We describe how we generated single photons for the experiment and explain how we obtained the physical design starting from the conceptual scheme. After discussing some technical issues we give the mathematical description of the physical setup.

In the fourth chapter we describe how we used the setup to acquire the data and how we processed the data to obtain the final result i.e. $-3.893(6)$ for the left hand side of the KCBS inequality, which lies 120 standard deviations below the classical bound of $-3.081(2)$. We also discuss the systematic effects and how we deal with them.

Introduction

In 1802, W. H. Wollaston observed dark lines in the otherwise continuous spectrum of the sun [13]. After describing them as boundaries between the colours, he abandoned the topic [14]. Twelve years later, the lines were rediscovered and given more attention by J. Fraunhofer [14, 15]. More than a hundred years later, after many other puzzling discoveries and theoretical developments, the spectral lines were explained with the help of quantum mechanics.

Even though it was born from experiments and very successful at explaining them, quantum mechanics was hard to accept as a fundamental theory because of its intrinsic randomness – an unprecedented feature, if taken to be a genuine one [16]. One could believe that the randomness was not a fundamental property of the world, and that there was a deeper theory which would relate to quantum mechanics just like classical mechanics relates to classical statistical mechanics. However, in 1960, E. Specker showed that quantum mechanics cannot be explained by such an underlying realistic theory [6]. His reasoning involved single three-level systems. In 1966, J.S. Bell reached the same conclusion. Both works have their root in Gleason's theorem. Bell moved on to consider composite systems and derived an inequality that could be tested in the laboratory[1]. He found that quantum mechanics violates an inequality that must be fulfilled by local realistic theories [2]. In 1967, Kochen and Specker published a refined proof of the incompatibility of quantum mechanics with non-contextual realistic theories for single three-level systems [7].

The theorems of Bell, Kochen, and Specker allow us to show that already the formalism of quantum mechanics implies the impossibility of certain hidden variable theories (e.g. local; non-contextual). It is not a question of interpretation. We are not forced to simply believe that an unperformed measurement has no value assigned to it. We can prove it using quantum mechanics, or even demonstrate it in the laboratory. Many experiments

[1] Bell's original inequality was derived for an idealised case. Clauser, Horne, Shimony, and Holt derived an inequality applicable to real experiments [17].

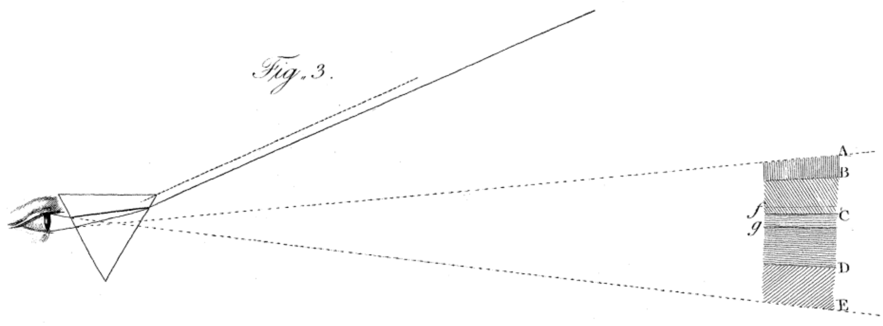

Figure 1: Sketch of Wollaston's method of viewing the solar spectrum (figure from [13]).

demonstrated this for the case of two qubits [4, 5, 10, 11]. We present the first experiment that employed a system that does not allow entanglement, while still disproving realistic theories[2] [12].

By performing experiments in the foundations of quantum mechanics we get closer to the intuitive understanding of the basic features of this theory, which have not been recognized until the works of Bell, Kochen, and Specker. If we are to observe new "dark lines in the continuous spectrum", it might be easier to notice that they contradict our currently accepted theories, not only quantitatively but even conceptually.

[2]in our case non-contextual

Chapter 1

Bell-Kochen-Specker theorem

The Heisenberg uncertainty principle teaches us that we cannot prepare an ensemble characterized by well defined position and momentum (or any other pair of conjugate variables). If we repeat a preparation procedure many times (in this way we create an ensemble) and measure position x or momentum p at each trial, then the standard deviations Δx and Δp fulfil the (uncertainty) relation $\Delta x \Delta p \geq \hbar/2$. The uncertainty principle, however, does not tell us anything about individual members of an ensemble. We might ask if the position and momentum are defined prior to the measurement. The fact that quantum mechanics does not allow us to predict the values of x, and p for an individual measurement does not answer this question either. We ask about the possibility of existence, not of being measured or even predicted [18]. Von Neumann answered this question in the negative [19], but his argument was found to be based on a dubious assumption [2]. J.S. Bell even called it silly and devised an argument free of this assumption. Kochen and Specker devised a similar argument that involves only a discrete, finite set of observables [7], whereas Bell's proof relied on a continuum of observables. Bell, Kochen and Specker proved that there is no way to assign values to quantum-mechanical observables in a non-contextual way. We call this result the Bell-Kochen-Specker (BKS) theorem. Our experiment realises measurements for which the predicions of quantum mechanics differ from those of non-contextual hidden variable theories.

In this chapter we will present the theoretical notions and results most relevant to our work: the BKS theorem in its various versions (special attention will be given to the version upon which our experiment is based [8]). In the first section we introduce the necessary concepts (1.1.1), discuss the background of the theorem, and finally formulate it. Later, we prepare the ground for the presentation of the proofs of the theorem. We focus on the three-dimensional Hilbert space (1.1.2). We present the origin of the BKS theorem (1.1.3), and discuss its relation to Bell's theorem [2]. In section 1.2 we explain what we mean by a BKS theorem and list the proposals and experiments rooted in the theorem. In the last section of this chapter, 1.3, we present the version of the BKS theorem due to Klyachko, Can, Binicioglu and Shumovsky (KCBS) including the derivation of the inequality, quantum violation, and generalizations [8].

1.1 Theoretical background and the formulation of the theorem

The BKS theorem states that quantum mechanics is in conflict with non-contextual hidden variable theories.

1.1.1 Setting the language

A hypothetical theory in which the values for individual un-performed measurements would exist is called a **hidden variable theory**. The relation of hypothetical hidden variable theories to quantum mechanics was sometimes said to be analogous to the relation between classical mechanics and classical statistical mechanics (e.g. [20] p. 672).

General hidden variable theories can be constructed that agree with quantum mechanics (QM) in all of their predictions and cannot be discerned from it [21]. Additional assumptions about the theories are required in order to make them distinguishable from QM. In other words, the assumption of values assigned also to unperformed measurements itself is not enough to lead to a conflict between QM and the hypothetical theory.

Since the hidden variable theories are supposed to "cure" the strangeness of QM, it is natural to demand from them the fulfilment of certain conditions which are naturally fulfilled in classical physics.

Realism is implicit in the idea of simple hidden variable models. It states that there exist values pre-assigned to measurements or in other words that even the unperformed measurements have results assigned to them.

To define **non-contextuality**, let us consider three observables: A, B, and C, with the following commutation relations: $[A, B] = [A, C] = 0$ and $[B, C] \neq 0$ (see Fig. 1.1). Assignment of a value to an observable A is called non-contextual if it is independent of the context of the measurement, that is, it is the same in the case when A is measured alone, together with B, or together with C.

Non-contextual realism states that one can map all the observables A_i onto real numbers, namely, there is a value assigned to each observable denoted by $v(A_i)$.

According to quantum mechanics, measurement results for an observable A belong to the spectrum (set of eigenvalues) of A (denoted by $\sigma(A)$). A hidden variable theory (HVT) is supposed to reproduce quantum mechanical predictions for measurement results so the value assigned by any HVT to an observable should also belong to its spectrum:

$$v(A) \in \sigma(A). \tag{1.1}$$

If $(A_1, A_2, A_3, ...)$ are commuting observables then quantum mechanics requires that the possible result of a joint measurement of $(A_1, A_2, A_3, ...)$ belongs to the set of their simultaneous eigenvalues. Any functional relation

$$f(A_1, A_2, A_3, ...) = 0, \tag{1.2}$$

fulfilled by the commuting observables has to be fulfilled by their simultaneous eigenvalues. For the hidden variable theory to agree with quantum mechanics one assumes that the values assigned to the commuting observables $(A_1, A_2, A_3, ...)$ also fulfil the relation

$$f(v(A_1), v(A_2), v(A_3), ...) = 0. \tag{1.3}$$

Sometimes special cases of the implication (1.2) $\Rightarrow$ (1.3) are introduced, called the **sum rule**

$$A_1 = A_2 + A_3 \Rightarrow v(A_1) = v(A_2) + v(A_3), \tag{1.4}$$

and **product rule**

$$A_1 = A_2 A_3 \Rightarrow v(A_1) = v(A_2)v(A_3), \tag{1.5}$$

where A_1, A_2, and A_3 commute.

The Bell-Kochen-Specker (BKS) theorem[1] states that quantum mechanics (QM) is not compatible with non-contextual hidden variable theories (NCHVTs) i.e. predictions of QM differ from those of NCHVTs. A Hilbert space of at least three-dimensions is required to exhibit the incompatibility.

[1] The Bell-Kochen-Specker theorem is commonly known as Kochen-Specker theorem, but Bell made a decisive step from Gleason's theorem to a statement about hidden variable theories [18].

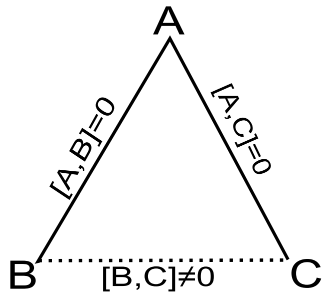

Figure 1.1: A diagram illustrating non-contextuality. Observables are depicted as vertices and the vertices corresponding to a pair of commuting observables are connected by solid lines. The value assigned to the observable A by a hidden variable theory, denoted by $v(A)$ is independent of the context of the measurement of A – the choice of the co-measured observable (B or C).

1.1.2 Bell-Kochen-Specker theorem for three-dimensional Hilbert space

Proofs in the three-dimensional Hilbert space are more general than those in higher dimensional spaces. They are at the same time proofs in any higher dimension, because an N-dimensional space can be taken to be a subspace of an (N+1)-dimensional space.

Representation of measurements by directions in 3D

For historical reasons, the proofs of the BKS theorem usually involve measurements that are conveniently expressed with spin components along certain directions. With such a representation one can visualise the measurements as directions in real three-dimensional space (Euclidian space). The measurements involved in BKS theorem proofs can usually be represented as $S_{\vec{n}}^2$ (squared component of spin along direction $\vec{n}$). The following holds true for such measurements:

$$\left[S_{\vec{n}}^2, S_{\vec{m}}^2\right] = 0 \Leftrightarrow \vec{n} \perp \vec{m}. \tag{1.6}$$

The above relation makes the representation with directions in a three-dimensional space convenient. It also allows one to turn the problem of finding a BKS set of directions into a purely geometric one. Commuting observables are represented by orthogonal directions.

Another important relation characterizing the measurements on spin-1

($s = 1$) systems is

$$S_{\vec{x}}^2 + S_{\vec{y}}^2 + S_{\vec{z}}^2 = s(s+1)I = 2I, \tag{1.7}$$

where $\vec{x}$, $\vec{y}$, and $\vec{z}$ represent orthogonal directions and I denotes the three-dimensional unit matrix. This relation has a simple physical interpretation for the case of spin-1 particles, but for the BKS theorem this is irrelevant. One can, instead, formulate a relation that holds true in any dimension of Hilbert space

$$\sum_{i=1}^{N} P_{\vec{n}_i} = I, \tag{1.8}$$

where $P_{\vec{n}_i}$ are projectors onto the basis vectors of an N-dimensional Hilbert space $\vec{n}_i$. This relation is sometimes called "decomposition of unity". It follows from 1.8 and 1.1 that

$$v\left(\sum_{i=1}^{N}(P_{\vec{n}_i})\right) = v(I) = 1. \tag{1.9}$$

Using the sum rule (1.4) and equation 1.9 we obtain

$$\sum_{i=1}^{N} v\left(P_{\vec{n}_i}\right) = v\left(\sum_{i=1}^{N}(P_{\vec{n}_i})\right) = 1. \tag{1.10}$$

Since the value assigned to each projector must be either 1 or 0 (condition 1.1), only one of the N projectors can be assigned 1 and the others must be assigned 0. This observation leads to a contradiction for some sets of projection operators (which are sometimes called Kochen-Specker sets). In other words, there is no way of assigning the values $v\left(P_{\vec{n}_i}\right)$ to all the projectors of a given set in a way satisfying the sum rule.

Representation of BKS sets of observables by two-dimensional diagrams

One can represent the observables involved in BKS theorem proofs by two-dimensional diagrams. Observables are depicted as vertices and the vertices corresponding to a pair of commuting observables are connected by lines. This means that, for example, a triangle on a BKS diagram corresponds to a triad of orthogonal directions (for the spin projection squared measurements) or to a triple of commuting observables. Note that there might be many diagrams in three dimensions having the same graph representation. The most famous example of a BKS diagram is the one found by Kochen and Specker, which contains 117 directions ([7]; Fig. 1.3) and was the first proof of the BKS theorem involving a discrete set of directions.

Value assignment to an observable translates to colouring the corresponding vertex of a diagram. We will focus on Hilbert spaces of dimension three and degenerate observables with two different eigenvalues. For diagrams this will translate to the use of two colours (commonly black and white are used).

Diagram	**Quantum mechanics**	**Space R³**
		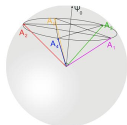
vertex Λ	observable $S^2_{\vec{n}}$	direction $\vec{n}$
straight line	commutativity $\left[S^2_{\vec{n}}, S^2_{\vec{m}}\right] = 0$	orthogonality $\vec{n} \perp \vec{m}$
colour ○ ●	value $v\left(S^2_{\vec{n}}\right)$	colour ○ ●

Figure 1.2: Correspondence between three ways of description of the BKS theorem: two-dimensional diagrams, quantum mechanical operators, directions in three-dimensional space.

1.1.3 Origin of the Bell-Kochen-Specker theorem

While considering alternatives to the way that expectation values are computed in quantum mechanics, i.e.

$$\langle A \rangle = Tr\left\{\rho A\right\}, \tag{1.11}$$

where ρ is a density operator describing a given preparation and A is a measured observable, Gleason found that under certain basic assumptions

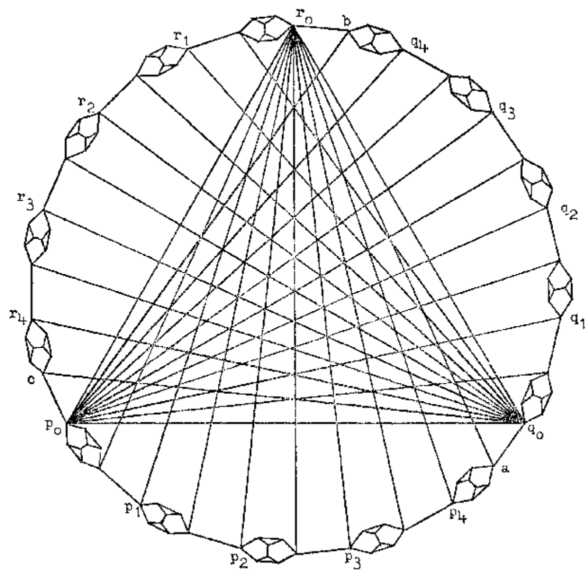

Figure 1.3: Diagram representing the directions that constitute the proof of the BKS theorem by Kochen and Specker [7]. Observables are depicted as vertices and the vertices corresponding to a pair of commuting observables are connected by lines (figure from [7]). It is not possible to assign values to all the observables at the same time in agreement with quantum mechanics.

there is no alternative to the formula 1.11 for Hilbert spaces of dimension higher than two. The main assumption is the strong superposition principle (any orthogonal basis represents a realisable maximal test, see page 54 in [22]). It is supplemented by reasonable continuity arguments.

Bell noticed that Gleason's result can be used to prove that there is no way to assign values to certain projectors such that the sum rule is respected [2]. He showed that Gleason's theorem implied that directions assigned 0 and 1 cannot be arbitrarily close. On the other hand, it follows from 1.1 that the only values assigned by hidden variable theories to the projectors are 0 and 1, and both of them have to occur because of 1.10. This implies that there are arbitrarily close projectors assigned different values, which contradicts the corollary of Gleason's theorem.

Although Bell was the first to find the conflict between quantum mechanics (QM) and non-contextual hidden variable theories [2], it was Kochen and Specker who found the first proof based on a finite set of directions [7]. Bell used a continuum of directions in his proof.

The BKS set of Kochen and Specker consists of 117 directions. Later smaller sets were found (e.g. [23, 24, 25, 26]). The smallest set was found by Cabello et al. They used only 18 directions in a four-dimensional Hilbert space [26]. Eighteen is proven to be the smallest number of directions required to form a BKS set [27].

In 2011, Yu and Oh found a state-independent proof of the Kochen-Specker (KS) theorem in three dimensions using only 13 rays [28]. They showed that a non-contextual hidden variable theory leads to new inequalities that are violated by quantum mechanics. One of the inequalities is based on the original KS assumption (sum rule) and involves only four rays from the 13-ray set explicitly. The second inequality involves all the 13 vectors explicitly but relaxes the assumption of the sum rule, leaving only the assumption of non-contextual realism. The result is important, because of the experimental possibilities it opens. All the previously-known state-independent inequalities for qutrits involved too many observables to be tested experimentally. The quantum violation of the inequalities found by Yu and Oh is big enough to be experimentally observed.

1.1.4 Relation between Bell and BKS theorems

Historically, Bell's theorem can be regarded as a step following the BKS theorem. Having found his proof of the impossibility of assigning definite values to the projectors in three-dimensional Hilbert spaces, which was free of von Neumann's dubious assumption, Bell turned his attention to the implicit assumption of non-contextuality he made in his proof.

> "That so much follows from such apparently innocent assumptions leads us to question their innocence." J.S. Bell [2]

Indeed, in light of Bohr's views, one should not expect the value of a measurement to be independent of the way it is measured. However, the proof that results independent of the measurement context cannot be assigned to projectors in agreement with quantum mechanics makes the issue no longer a matter of views.

Bell wanted to replace the assumption of non-contextuality with a more physical one. He turned to locality, which loosely speaking means that the results of an experiment in a given space-time region cannot depend on the measurement settings or results in a space-like separated space-time region. Locality is a weaker assumption than non-contextuality. Non-contextual theories are a subset (special case) of local realistic theories. It follows that every proof of Bell's theorem proves also the BKS theorem. The converse is not, in general, true. Not every BKS proof can be turned into a Bell proof. In [29] Mermin gives an example of such a proof (known as Mermin-Peres square; see Fig. 1.4), where assuming locality is not enough to find the contradiction (one needs to assume non-contextuality). In the same article he describes another set of observables (known as Mermin star; see Fig. 1.5), this time in eight-dimensional Hilbert space, which constitutes a proof of the BKS theorem and at the same time can be used to prove the Bell theorem when the predictions of quantum mechanics for a Greenberger-Horne-Zeilinger (GHZ) state are used.

This allows for a direct comparison of the two theorems. In the original Bell argument, statistical predictions were involved, making it different from the BKS theorem, where the assignment of definite values is impossible without the need to consider statistical distributions of the measurement results. Bell's theorem in its GHZ version is closer in form to the BKS theorem.

σ_x^1	σ_x^2	$\sigma_x^1\sigma_x^2$
σ_y^2	σ_y^1	$\sigma_y^1\sigma_y^2$
$\sigma_x^1\sigma_y^2$	$\sigma_x^2\sigma_y^1$	$\sigma_z^1\sigma_z^2$

Figure 1.4: Mermin-Peres square. A set of observables constituting a BKS theorem proof in four- (and higher) dimensional Hilbert space (figure from [18]). σ_i^j represent the i-th Pauli matrix of the j-th subsystem ($i \in \{x, y, z\}$ and $j \in \{1, 2\}$). Observables in each row and column of the table commute. The product of the observables in all the rows and columns are $+1$ except for the last column where the product is -1. This observation implies that it is not possible to assign values to all the observables in agreement with the product rule (1.5).

1.2 Proposals and experiments that followed

While the theorem of Bell, Kochen and Specker is a mathematical statement about quantum mechanics and a class of theories alternative to it (non-contextual hidden variable theories), one might still ask if the predictions of quantum mechanics used in the derivation of the theorem can be experimentally tested. Such a test would allow one to discriminate between the two alternative descriptions with the help of an experiment.

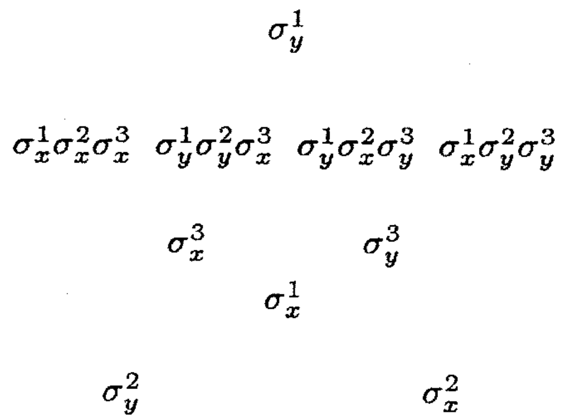

Figure 1.5: Mermin star. A set of observables constituting a BKS theorem proof in eight- (or more) dimensional Hilbert space (figure from [18]). σ_i^j represent the i-th Pauli matrix of the j-th subsystem ($i \in \{x, y, z\}$ and $j \in \{1, 2, 3\}$). Observables lying at each edge of the star commute. The product of the observables in each such group is $+1$ except for the horizontal line with triple products of observables where the product is -1. This observation implies that it is not possible to assign values to all the observables in agreement with the product rule (1.5).

1.2.1 BKS experiments

Photon experiment 2003

The proposal of Simon et al. [30] based on the proof by Cabello et al. [26] was realised by Huang et al. [31]. An optical interferometric setup was used to realise the required measurements on heralded single photons.

Neutron experiment 2009

Cabello derived a Bell-like inequality using observables from the Mermin-Peres proof that could be used for a BKS experiment with neutrons [9]. The proposal was realised with the help of a neutron interferometer in which entangled states of neutron's path and spin were prepared and analysed [32].

State-independent inequality

In 2008, Klyachko, Can, Binicioglu and Shumovsky (KCBS) found a proof of the BKS theorem that involved only five measurements. Later it was generalized by Cabello [9]. In the same article Cabello presents an inequality based on the 18-direction set [26] and another based on the Mermin-Peres square [29], (p.189 in [22]). Remarkably, the inequalities found by Cabello are violated by all states in four-dimensional Hilbert spaces, whereas the KCBS inequality is not violated by all the states in three-dimensional Hilbert space. Cabello's inequality was tested in experiments with ions [10] and photons [11]. It was also generalised to higher-dimensional Hilbert spaces [33].

Ion experiment 2009

In the experiment with ions, Kirchmair and co-workers performed sequences of three measurements on pairs of qubits [10]. This was possible thanks to a non-demolition measurement technique. Sequential measurements, however, open the so-called compatibility loophole [34]. The measurements were performed on various states, including the maximally mixed state.

Photon experiment 2009

In the photonic experiment by Amselem et al. [11] the same inequality was tested, but a different approach to measuring sequences of observables was taken. The experiment used an idea that was first described by Simon et al. [30] where a cascade of measurement devices was used to sort the particles leaving the entire setup according to the results of the measurement series performed on them – the setup was analogous to a cascade of differently oriented Stern-Gerlach apparatus. The experiment was performed with the help of an attenuated laser diode. The measurement apparata were assumed to be identical when they were built in the same way. There were also connections between the boxes which were assumed not to change when being (dis-)connected.

1.2.2 Generalized "contextuality" and its applications

Spekkens generalized the notion of non-contextuality such that it can be applied to a broader class of hidden variable theories (not only deterministic ones) and not only to measurements, but also to preparations and transformations [35]. He proved analogues of the BKS theorem for the generalized non-contextuality, which, in contrast to the standard BKS theorem, applies also to qubits. He showed that it is equivalent to generalized negativity of quasi-probability distributions [36]. Spekkens et al. found that quantum mechanics out-performs non-contextual (as defined by Spekkens) theories at parity-oblivious multiplexing [37].

1.3 KCBS version of Bell-Kochen-Specker theorem

In this section we will present the version of BKS theorem on which we based our experiment.

In 2008 Klyachko, Can, Binicioglu and Shumovsky (KCBS) found an inequality that is violated for certain states of single qutrits [8]. Remarkably, the inequality involves only five measurements and the violation predicted by quantum mechanics is relatively large, which is crucial for experimental tests.

1.3.1 Derivation of the KCBS inequality

Algebraic inequality

Consider a function, $K(a_i) = a_1a_2 + a_2a_3 + a_3a_4 + a_4a_5 + a_5a_1$, where the $a_i = \pm 1$ and $(i = 1, 2, ..., 5)$. To find its minimal value, we wish to choose the a_i to make as many terms as possible equal to -1. We can succeed for the first four terms by choosing alternating values of $+1$ and -1, but then, whatever value we choose for a_1 to start the sequence, we are left with $a_1 = a_5$, thus making the fifth term equal $+1$. Similarly for any other sequence, there is at least one term equal $+1$. Consequently, $K(a_i) \geq -3$ for all choices of a_i's:

$$a_1a_2 + a_2a_3 + a_3a_4 + a_4a_5 + a_5a_1 \geq -3. \tag{1.12}$$

Derivation using the assumption of non-contextuality

According to a non-contextual hidden variable model, each of the five measurements A_i has a pre-defined value $v(A_i)$ independent of the context of the measurement (the co-measured observable) e.g. $v(A_2)_{A_1} = v(A_2)_{A_3}$. This is true for each member of an ensemble, so we can move from the inequality for the individual values 1.12 to an inequality for averages:

$$\langle A_1A_2\rangle + \langle A_2A_3\rangle + \langle A_3A_4\rangle + \langle A_4A_5\rangle + \langle A_5A_1\rangle \geq -3, \tag{1.13}$$

where the angle bracket denotes averages over a statistical ensemble and does not imply a quantum-mechanical expectation value.

In the article by KCBS the authors claim that the violation of the inequality shows the conflict between quantum mechanics and hidden variable theories which need not be non-contextual. If one uses the definition of non-contextuality that we used (also used in most of the literature), this statement is false. The proof by KCBS does rely on the assumption of non-contextuality.

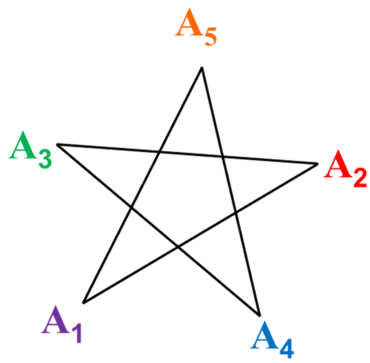

Figure 1.6: BKS diagram of the KCBS proof with five pairs of commuting observables [8]. Observables are depicted as vertices and the vertices corresponding to a pair of commuting observables are connected by straight lines. This diagram, in contrast to the original diagram by Kochen and Specker [7], is colourable – there is a way to assign values to the observables in a way satisfying the sum rule. The conflict between non-contextual realism and quantum mechanics arises when statistical predictions for specific states are considered.

1.3.2 Quantum mechanical violation of the KCBS inequality

Above we rederived the KCBS inequality which involves five pairs of observables (the pairs need to commute). This translates to five pairs of pair-wise orthogonal directions $\vec{l}_i, \vec{l}_j$ if we consider observables of the form $S^2_{\vec{l}_i}$.

Such a set of directions was found by KCBS and can be described as follows (see Fig. 1.7). Take a sphere, inscribe a circle in it, inscribe a regular pentagram into it. Connect the vertices of the pentagram with the centre of the sphere. There is a position of the circle on the sphere such that the lines connecting the neighbouring vertices with the centre are orthogonal to each other. They define the five directions:

$$\vec{l}_i = R_{\frac{4\pi}{5}}^{i-1} \begin{pmatrix} \sqrt{\frac{1}{10}\left(5-\sqrt{5}\right)} \\ \sqrt{\frac{1}{10}\left(5-\sqrt{5}\right)} \\ \frac{1}{5^{1/4}} \end{pmatrix}, \tag{1.14}$$

where $i \in 1, 2, ..., 5$ and $R_{\frac{4\pi}{5}}$ represents the rotation about the z axis (the five-fold symmetry axis of the pentagram), and is given by the following matrix:

$$R_{\frac{4\pi}{5}} = \begin{pmatrix} \frac{1}{4}\left(-1-\sqrt{5}\right) & -\frac{1}{2}\sqrt{\frac{1}{2}\left(5-\sqrt{5}\right)} & 0 \\ \frac{1}{2}\sqrt{\frac{1}{2}\left(5-\sqrt{5}\right)} & \frac{1}{4}\left(-1-\sqrt{5}\right) & 0 \\ 0 & 0 & 1 \end{pmatrix}. \tag{1.15}$$

The directions $\vec{l}_1, \vec{l}_2, ..., \vec{l}_5$ define the five observables $A_1, A_2, ..., A_5$, by the relation

$$A_i = 2S_{\vec{l}_i}^2 - I = I - 2|\vec{l}_i\rangle\langle\vec{l}_i|. \tag{1.16}$$

The operator $S_{\vec{l}_i}^2$ has 0 and 1 as its eigenvalues and for the inequality we need ± 1 – this is the reason for the scaling and shifting used in 1.16.

Having defined the measurements we can start testing the inequality with the state given by the symmetry axis of the pentagram. To find a numerical prediction of quantum mechanics let us recast the KCBS inequality into a geometric form (using 1.16):

$$\sum_{i\ mod\ 5} |\langle\vec{l}_i|\vec{k}\rangle|^2 \leq 2, \tag{1.17}$$

where $\vec{k}$ represents the pure input state (vector). For the symmetry axis state

$$\vec{\Psi}_0 = \begin{pmatrix} 0 \\ 0 \\ 1 \end{pmatrix}, \tag{1.18}$$

we obtain

$$|\langle\vec{l}_i|\vec{\Psi}_0\rangle|^2 = cos^2\widehat{l_i\Psi_0} = \frac{1}{\sqrt{5}}, \tag{1.19}$$

which provides violation of the KCBS inequality $\sum_{i\ mod\ 5} |\langle\vec{l}_i|\vec{\Psi}_0\rangle|^2 = \sqrt{5} > 2$. The geometry described above provides the maximal violation of the inequality in three-dimensional Hilbert space [38].

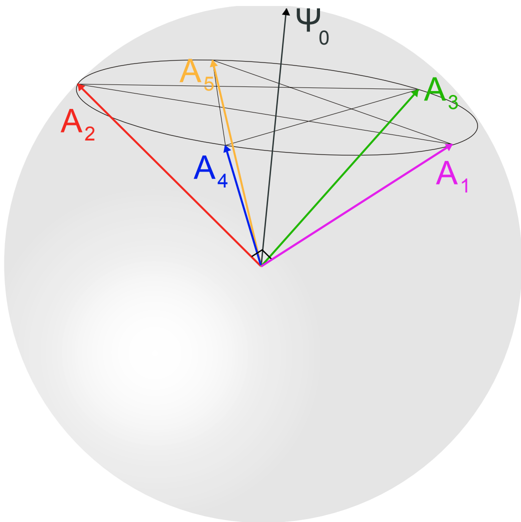

Figure 1.7: Representation of the measurements and a state providing maximal violation of the Klyachko, Can, Binicioglu and Shumovsky (KCBS) inequality 1.13 as directions in three-dimensional space. The directions along which squared spin components are measured are labelled by the corresponding measurements A_i ($i = 1, 2, ..., 5$). They are given as $2S^2_{\vec{l}_i} - 1$, where $S^2_{\vec{l}_i}$ is a spin projection onto the direction $\vec{l}_i$. The measurements directions are pair-wise orthogonal, making the measurements A_i pair-wise compatible (see 1.6). These five pairs correspond to the five measurement devices from Figs 2.5b-f. For a maximal violation of the KCBS inequality, the points where the directions intersect the sphere form a regular pentagram and the input state $\vec{\Psi}_0$ has zero spin along the symmetry axis of the pentagram. The directions can be also viewed as direct representation of the vectors in Hilbert space. Here we only use vectors with real coefficients and so the three-dimensional Hilbert space turns into a three-dimensional Euclidean space which is convenient for visualisation and calculations.

1.3.3 Properties of the KCBS proof and its generalizations

Brief summary

1. Three is the minimal dimension of Hilbert space in which BKS theorem proofs can exist.
2. Five is the minimal number of observables that lead to a violation of a non-contextual hidden variable theories (NCHVTs) inequality in three-dimensional Hilbert spaces [39, 40].
3. Violation of the KCBS inequality for N-grams ($N > 5$) occurs only for odd N and is smaller than the violation for $N = 5$ [39, 41, 40, 38].
4. The regular pentagram is the optimal shape for the violation of the KCBS inequality, but every non-degenerate pentagram provides a violation for some states [39, 41, 38].
5. The optimal state (vector) points along the five-fold symmetry axis of the pentagram. Vectors making an angle smaller than approximately $31°$ with the symmetry axis of the pentagram also violate the inequality [39, 41, 38].

Minimal dimension of Hilbert space

A single qutrit is the simplest system for which a BKS theorem proof can be found. Hilbert space of a single qubit has two dimensions. It follows that for each projector (ray) in such a space there is only one commuting projector (orthogonal ray). This means that each projection can have only one context, and as a consequence, one cannot construct any non-degenerate BKS diagram.

Minimal number of measurements

It was shown by Klyachko [39] and later by Cabello [40] that five is the minimal number of observables that lead to a violation of a NCHVT inequality in three-dimensional Hilbert spaces.

Any two-outcome observable with possible results -1 or $+1$ on a qutrit system must be represented by a 3×3 matrix with eigenvalues -1 and $+1$, one of them degenerate. Without the loss of generality we can assume that the two-outcome observables are of the form

$$A_i = 2|\vec{l}_i\rangle\langle\vec{l}_i| - I. \tag{1.20}$$

If we take three pair-wise commuting observables we obtain three pair-wise orthogonal directions and they constitute an orthogonal triad. It follows that all three observables commute with each other – they are measurable by a single experimental setup.

If we consider four measurements we can show that there is no non-degenerate set of directions characterized by the required orthogonality relation:

$$\vec{l}_1 \perp \vec{l}_2 \perp \vec{l}_3 \perp \vec{l}_4 \perp \vec{l}_1. \tag{1.21}$$

Let us start from the vector $\vec{l}_1$. It defines a plane in which $\vec{l}_2$ and $\vec{l}_4$ lie. Each of the two vectors however also defines a plane in which $\vec{l}_3$ has to lie. As a result $\vec{l}_3$ has to lie at the intersection of the two planes, which in turn happens to point along $\vec{l}_1$. This means that we cannot arrange four directions in the desired way. We end up in the case of an orthogonal triad, for which the three corresponding projectors commute, so there is no chance for a contradiction between quantum mechanics and hidden variable theories.

Minimal number of co-measured observables

In the KCBS proof only pairs of observables are involved, whereas the Cabello inequality and experiments based upon it involved correlations of triples of measurements. Paired observables represent the simplest possible case, since for single observables one cannot use the assumption of non-contextuality (or locality) to derive a non-trivial inequality.

Optimal number of vertices

In an unpublished work KCBS show that for higher odd numbers of vertices there is a violation, but it is smaller than for pentagrams [39, 41]. They also conjecture that there is no violation of a generalized inequality for even numbers of vertices.

Optimal geometry of projectors and state

It was shown that for the regular pentagram, the state lying at its symmetry axis (Ψ_0) provides the maximal violation. States represented by real vectors also give a violation as long as the angle between them and the symmetry axis of the pentagram is less than approximately 31° (see Fig. 1.8 and [39, 41, 38]).

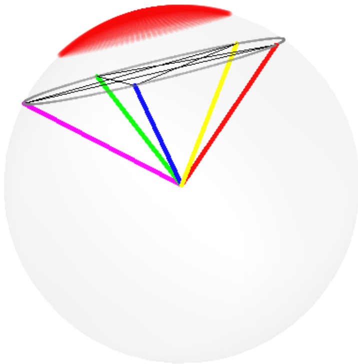

Figure 1.8: Subset of states which violate the KCBS inequality. Vectors connecting the centre of the sphere with the red region at the top of the sphere provide a violation of the KCBS inequality 1.3. Note that the vectors constituting the pentagram do not provide a violation of the KCBS inequality, when used as inputs for the measurements.

1.4 BKS theorem for finite precision measurements

The feasibility of a BKS experiment has been a subject of a long debate. Meyer started the discussion by claiming that finite experimental precision nullifies the BKS argument [42]. He pointed out that real experiments cannot distinguish a dense subset from its closure and that the rational vectors which are dense in S^2 (two-dimensional sphere) can be coloured in agreement with the sum rule (only one out of the three orthogonal projectors in three-dimensional Hilbert space is assigned the value 1, while the remaining two are assigned 0). Meyer concluded that the BKS argument has no connection to real experiments. While the mathematical results of Meyer were not questioned, their interpretation was.

1.4.1 Meyer's nullification of the BKS theorem for real experiments

Meyer based his argument [42] on the following three observations:

1. Vectors with rational coordinates ($S^2 \cap \mathbb{Q}^3$) can be coloured in agreement with the sum rule. This means that there exist colourable diagrams of observables arbitrarily close to the BKS diagrams for spin-1

systems.

2. Rational vectors $S^2 \cap \mathbb{Q}^3$ are dense in S^2.

3. Real experiments cannot distinguish a dense subset from its closure.

According to Meyer, the conjunction of (1), (2), and (3) implies that the BKS theorem does not apply to real measurements. This implication seems to be the root of the controversies [43, 44, 45, 46, 47, 48].

Kent generalises Meyer's result from spin-1 systems to arbitrary finite-dimensional systems and from projective measurements to positive operator valued measurements [49].

Clifton and Kent construct a non-contextual model which according to its authors can reproduce the quantum mechanical predictions for finite-precision measurements [50].

1.4.2 Counterarguments to the nullification

In the present subsection we will give a brief account of the arguments against Meyer's nullification of BKS.

Mermin pointed out that the continuity of the quantum mechanical probabilities under slight changes of the experimental configurations implies that even finite precision experiments would allow one to observe results contradicting NCHVTs [43]. Morover, Meyer's colourable sets cannot fully reflect the commutativity of the uncolourable diagram. This is a consequence of the BKS-theorem. The uncolourability is a consequence of the topology. If the topology was faithfully mapped from the BKS diagrams to Meyer's diagrams the latter would remain uncolourable. In other words, at least one connection of a BKS diagram is missing in each of Meyer's diagrams, and this makes them colourable. This observation tells us that compatibility of the co-measured observables is crucial for the BKS argument.

Larsson [46] and independently from him Simon, Brukner, and Zeilinger (SBZ) [44] took an operational approach that assumes little about the theoretical model. They defined the observables by the settings of the "knobs" on the measurement apparatus, which itself is a "black box". To derive a BKS inequality, SBZ used a set theory argument. They found that imperfect measurements and preparations still allow one to observe a conflict with non-contextual realism for sufficiently high (but finite) precision. The threshold precision depends on the number of transformations needed to traverse the BKS diagram used.

Cabello also claimed that BKS experiments are feasible [47]. He demonstrated that the model of Clifton and Kent [50] leads to predictions which are in conflict with quantum mechanics. He derives an inequality fullfiled by NCHVTs and violated by quantum mechanics.

Appleby and Havlicek point out that the value assignment in the Clifton-Kent (CK) models is such that in every neighbourhood, one can find the two possible truth values [45, 48, 51]. Appleby and Cabello show that such dense discontinuities are a necessary feature of CK models [47, 45, 48]. CK do not question those findings.

1.4.3 Answer to the counterarguments

In [52] Barrett and Kent defend Meyer's position. They scrutinize the definitions of (non-)contextuality used by the critics of Meyer and question their justifiability. They point out that classical mechanics can be found contextual according to the SBZ definition. Later they point out the interpretation problems of BKS experiments. They postulate that the physical realisation of the experiment has to be analysed in detail to find out what theories a given experiment disproves. This is because none of the experiments is free from tacit assumptions about what is actually measured. Some experiments even rely on elements of quantum-mechanical formalism. If one accepts the formalism of quantum mechanics then, by the BKS theorem, no non-contextual model is possible, so the experiments seem unnecessary.

Meyer contrasts the Bell-CHSH inequality with the BKS theorem in their applicability to finite precision measurements. Barrett and Kent state that the finite precision does not pose problems for Bell-CHSH whereas it does so for BKS experiments [52]. It is an interesting question whether a different finite precision argument can be raised against Bell experiments.

1.4.4 Non-contextuality inequalities and their experimental tests as counterarguments to the nullification

The KCBS and Cabello's inequalities, that we discussed in the previous sections, were derived using only the assumption of non-contextual realism [8, 9]. Together with their quantum mechanical violation the inequalities constitute proofs of the BKS theorem. Neither the observables nor the states need to be precisely set for the violation to be observed – the violation of the inequalities is robust. This seems to constitute a strong argument against Meyer's claim of nullification already at the theoretical level. Interestingly, the violation of inequalities was even observed experimentally. Experimental violations of non-contextuality inequalities constitute yet another contribution to the discussion started by Meyer [10, 11, 12].

We show in the next chapter that it is possible to traverse a BKS diagram always keeping the pairs of co-measured observables compatible. One can even assure that the connections from a diagram are realised (the edges of the graph meet at the vertices) in the experiment for all but one connection.

Chapter 2

Concept of the experiment

This chapter takes a step, from mathematics, to physics. We show how a simple optical system can realise the geometry of a Bell-Kochen-Specker (BKS) proof [12]. From among the BKS proofs described in the previous chapter we have chosen the Klyachko, Can, Binicioglu and Shumovsky (KCBS) version [8] because of its simplicity (see section 1.3). The KCBS proof involves only a three-dimensional Hilbert space – the smallest possible (1.3.3), and only five different measurements – the minimum number in three-dimensional Hilbert space (1.3.3). Three-dimensional Hilbert space cannot be represented as a tensor product of two spaces, so entanglement cannot be defined for it (in our article [12] we call a system whose states belong to such a space indivisible).

Entanglement has been central to manifestations of "quantumness" since the beginning of the quantum theory. It is present in many quantum information processing protocols. Our work is in part motivated by the interesting question whether there are tasks where other features of quantum mechanics besides entanglement would allow one to outperform the classical protocols.

The Bell-Kochen-Specker theorem, in contrast to the Bell theorem, does not relate to properties of special quantum states. It relies on the algebra of observables instead. There have been BKS experiments performed with separable and even maximally mixed states [10, 11]. However, to our knowledge, all of the experiments involved pairs of qubits or systems described by other Hilbert spaces that allow for entanglement and as such would also allow a Bell-type experiment. Here we demonstrate the non-classicality (here, impossibility of a non-contextual hidden variable theory) of a system that does not allow entanglement.

2.1 Optical realisation of the KCBS geometry

To perform an experiment testing the KCBS inequality, we needed a three-level system (a qutrit). We used a single photon distributed among three modes (paths) to realise this. It has been shown that, if such an encoding is used, any unitary transformation can be realised with the help of phase-shifters and beam splitters only [53]. In this respect, encoding the state in path is more convenient than in energy or transverse mode of a photon, where it is not a trivial task to realise arbitrary unitary transformations.

Zukowski, Horne, and Zeilinger suggested a BKS experiment using path-encoding [54]. Although their proposal was a starting point of our project, we found a different scheme based on path-encoding that we present below. In section 2.3 we introduce the idea and describe path-encoding mathematically. In the next section (2.4) we show how this architecture can be used to realise the KCBS measurements.

The vertices alone do not constitute a BKS diagram: the connections between them are also necessary. Therefore, not only do we want the physical system to realise each measurement separately, but the entire structure of measurements to be mapped onto different configurations of the setup. With this in mind we construct our apparatus step by step, at the same time traversing the diagram. Every connection on the diagram has a counterpart in the physical setup. In a real experiment, we can never perform the desired measurements perfectly, because the setup is always slightly misaligned. For the BKS argument, however, it is not the exact measurements that matter, but their mutual relations (commutativity) and even more importantly the invariance of a single measurement while its context is altered. One can translate those demands into the language of diagrams. Commutativity means that two vertices are connected by a line. Keeping one measurement fixed in two contexts means that two lines, which represent the pairs of measurements, have one common end. In section 2.4 we describe how we ensure that these requirements are met by the experiment.

2.2 Logic of our argument

We use an inequality derived from the assumption of non-contextual realism (or equivalently, the existence of a joint probability distribution of the measurements involved). We use quantum mechanics (QM) to guide us in building an apparatus that should allow us to observe a violation of the inequality. If the experimental results violate the KCBS inequality we confirm the prediction of QM and at the same time disprove the hypothesis of non-contextual realism (the existence of a joint probability distribution of the measurements involved).

2.3 Photonic states encoded in path

Encoding

The physical system that we work with is a single photon propagating in three modes. Each mode is assigned a state vector. The modes can be distinguished perfectly, so the vectors $|a\rangle$, $|b\rangle$, and $|c\rangle$ that we assign to them have to be orthogonal. They constitute a basis of the Hilbert space describing a single photon distributed among three modes, so every state of such a photon can be described by a superposition: $\alpha|a\rangle + \beta|b\rangle + \gamma|c\rangle$. The orthogonality of the state vectors is crucial for the experiment, because it guarantees the commutativity of the corresponding projectors.

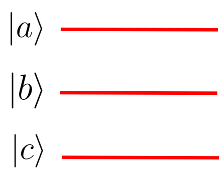

Figure 2.1: Three optical spatial modes with the assigned state vectors. The modes can be distinguished perfectly, so the vectors that we assign to them must be orthogonal. They constitute a basis of the Hilbert space describing a single photon distributed among three modes.

Transformations

Transformations can be conveniently performed on path-encoded systems with the help of phase-shifters and beam splitters, which couple the two modes they act upon (see Fig. 2.2). Mathematically, the action of a lossless two-mode beam splitter can be described by a unitary matrix (see e.g. [55]). The matrix representing a lossless symmetric beam splitter characterized by the amplitude reflectivity r is given by:

$$U_{BS} = \begin{pmatrix} r & -\sqrt{1-r^2} \\ \sqrt{1-r^2} & r \end{pmatrix}, \tag{2.1}$$

which is the same as a matrix representing a two-dimensional rotation by an

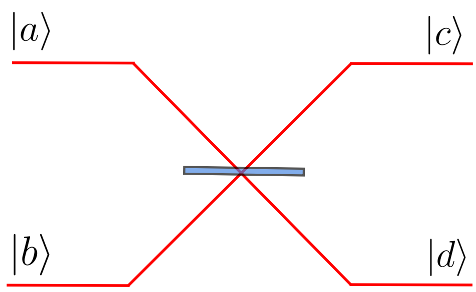

Figure 2.2: An optical beam splitter (BS) coupling two modes. If the modes are assigned vectors, the action of the BS can be described as a rotation in the plane spanned by the vectors $|a\rangle$ and $|b\rangle$. The rotation leads to a new basis: $\{|c\rangle, |d\rangle\}$.

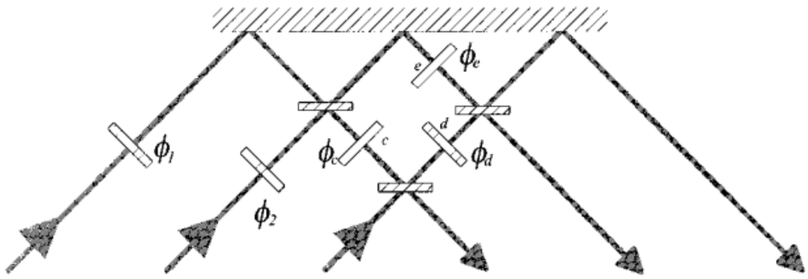

Figure 2.3: An example of an optical multiport in three-dimensional Hilbert space. A multiport is a generalisation of a beam splitter from two-dimensional to N-dimensional Hilbert space (two to N modes). It was shown that such a setup is sufficient to realise an arbitrary unitary operation in N-dimensional Hilbert space if tunable beam splitters and phase-shifters are used [53] (figure from [54]).

angle α, where $\alpha = arccos(r)$:

$$R(\alpha) = \begin{pmatrix} \cos\alpha & -\sin\alpha \\ \sin\alpha & \cos\alpha \end{pmatrix}. \tag{2.2}$$

The second optical component required to construct arbitrary unitary operations is a phase-shifter. It can be represented by the folowing matrix:

$$U_{PS}(\phi) = \begin{pmatrix} 1 & 0 \\ 0 & e^{i\phi} \end{pmatrix}. \tag{2.3}$$

In our experiment there are three modes involved, so transformations are described by 3×3 matrices. The KCBS proof of the BKS theorem involves only directions in real three-dimensional space (Euclidean space), so it is sufficient to consider rotations in such space.

An arbitrary rotation in 3D can be decomposed into three 2D rotations called Euler rotations (p. 171 in [56]). Such a decomposition is natural for our setup. The "rotation axis" is the mode which is not affected by a given transformation.

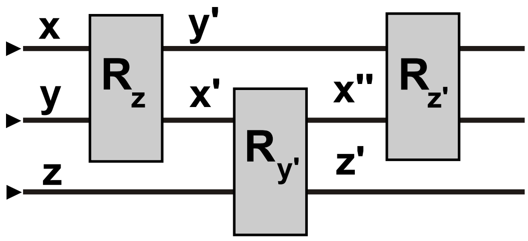

Figure 2.4: Euler's decomposition of an arbitrary rotation in three-dimensional Euclidean space realised by beam splitters acting on pairs of modes in a three-beam optical system.

Arrangements in the form of Fig. 2.4 are not the only setups which may be described by rotations. Since rotations in 3D form a group, any combination of rotations is also a rotation. This means that an arbitrary combination of beam splitters acting on three modes can be described as a three-dimensional rotation[1].

The result of Reck et al. [53] can be viewed as a generalization of Euler's rotation decomposition from three-dimensional Euclidean space to N-dimensional Hilbert space. There is a striking similarity between the setup obtained as a translation of Euler rotations into optics (see Fig. 2.4), performing arbitrary rotation in three-dimensional Eucilidian space, and the multiport performing arbitrary unitary operation in three-dimensional Hilbert space. Only phase-shifters need to be added to the former to turn it into a general multiport (see Fig. 2.3).

In order to perform a BKS experiment it is sufficient to use the setup in Fig. 2.4, composed only of tunable beam splitters, since all the important BKS diagrams for qutrits "live" in three-dimensional Euclidean space. We do not need to employ the result of Reck et al. [53], we can rely on the Euler rotations.

[1] For simplicity we assume that a beam splitter introduces no relative phase between the two modes it acts upon.

Measurement

Inherent in the path encoding is the ease of performing a measurement. Each mode is monitored by a single-photon detector (which mathematically can be described as a projection onto the state assigned to the mode the detector monitors). For other encodings one usually needs to split the modes into separate paths with the help of an extra component (e.g. prism, polariser) before the detection. For some encodings (e.g. using transverse modes of light) there is no standard device performing this task.

2.4 KCBS experiment with photonic qutrits

As discussed, path-encoding is our method of choice to map the Hibert space vectors $\vec{l_i}$ to the optical modes a photon can occupy. This naturally leads to the physical realisation of projective measurements $P_{\vec{l_i}} = |\vec{l_i}\rangle\langle\vec{l_i}|$ by detectors monitoring three modes.

The single-photon source provides us with a photon in a well-defined spatial mode. This is the starting point of our setup. At the other end of it we have detectors monitoring three distinct modes. In our experiment we planned to prepare the state providing the maximal violation of the inequality. One can see from the KCBS diagram 1.7 that this state does not belong to any measurement basis involved in KCBS inequality: it is not a part of the pentagram. Two rotations are required to transform the vector $\vec{Psi_0}$ (together with the orthogonal vectors with which it constitutes the basis), such that two of the original vectors are mapped onto $\vec{l_1}$ and $\vec{l_2}$. Preparation is depicted in 2.5.a, tunable beam splitters T_A, T_B realise the rotations.

To test the KCBS inequality we need to be able to perform two-outcome measurements on our system. We define the measurement outcomes in the following way: If a detector clicks we assign -1 to the corresponding observable, if it does not click we assign $+1$ to it. The measurements A_i defined in this way can be expressed with the help of projection operators: $A_i = I - 2|\vec{l_i}\rangle\langle\vec{l_i}|$.

Figs. 2.5b-f shows five different configurations of the measurement setup used to measure the five terms of the KCBS inequality 1.3. When moving from the setup depicted in Fig. 2.5.b to that of Fig. 2.5.c, we apply a transformation to the upper two modes and leave the lowermost mode untouched. The crucial property of our experiment is that we physically keep one of the measurements unchanged when moving between the terms of the inequality. Mathematically this can be described by a rotation whose axis is the vector assigned to the unaffected mode.

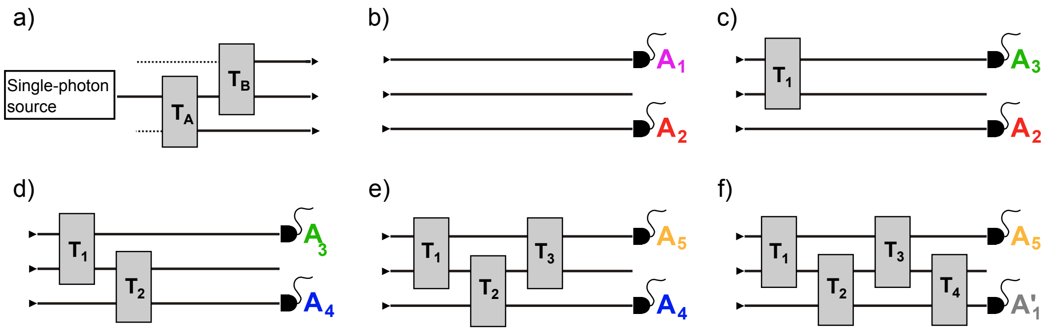

Figure 2.5: The conceptual scheme of the experiment with the preparation and five successive measurement stages [12]. Straight, black lines represent the optical modes (beams), gray boxes represent transformations on the optical modes. a) Single photons are distributed among three modes by transformations T_A and T_B. This preparation stage is followed by one of the five measurement stages. b-f) At each stage, the response of two detectors monitoring the optical modes defines the measurements as appearing in inequality 1.3. Outcomes of the measurements are defined by asking, "did the corresponding detector click?". If a detector clicks (does not click), then a value of -1 $(+1)$ is assigned to the corresponding measurement. A key aspect of our experimental implementation is that each transformation acts only on two modes, leaving the other mode completely unaffected. Thus, the part of the physical setup corresponding to the measurement of A_2 is exactly the same in the insets b and c (likewise A_3 is the same in the insets c and d, etc.). Note that this setup can also be arranged so that the choice between A_1 and A_3 is made long after A_2 is measured. Thus it appears reasonable to assume that the measurement result for A_2 is independent of whether it is measured together with A_1 or A_3. The same reasoning can be applied to the measurements A_3, A_4, and A_5.

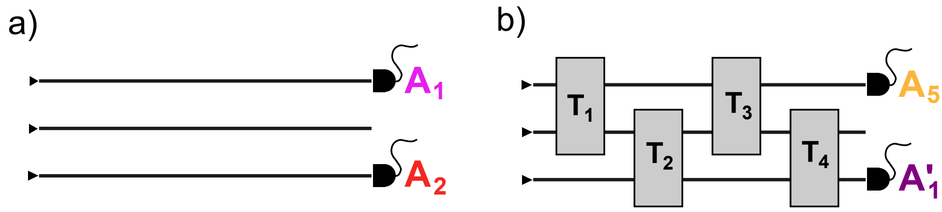

Figure 2.6: Loose-ends problem: setups used to measure $\langle A_1 A_2 \rangle$ and $\langle A_5 A_1' \rangle$.

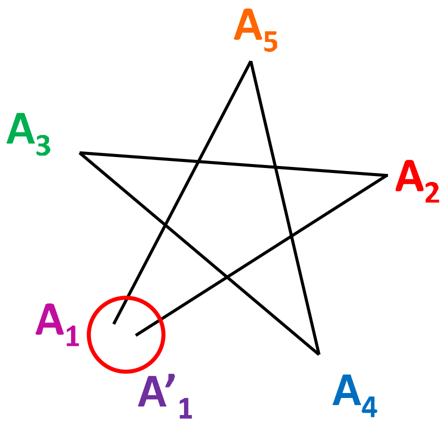

Figure 2.7: A simplified picture of the geometry of the loose-ends problem. The identity of the measurements A_1 and A_1' is not guaranteed by the construction. Furthermore, the imperfections of the transformations can accumulate and lead to the mismatch of A_1 and A_1'.

To move between the further terms of the inequality, we keep rotating the basis in the same way, always keeping one of the measurements (vectors we project onto) unchanged. After the last rotation, which should bring us back to the basis from which we started, we end up with the setup depicted at Fig. 2.5.f.

2.5 Loose-ends problem and its solution

The last measurement is not physically the same as A_1 (see 2.6). They would be identical in the ideal case where the transformations were performed perfectly, but even in this case, these would be two different realisations of the same projector. Therefore we call the final measurement A_1'. If we write down the KCBS inequality and replace the A_1 in the last term with A_1' the inequality becomes invalid. We need to modify it.

It is straightforward to modify the inequality such that a non-trivial bound can be found. We only need to fix the lack of connection between A_1 and A_1'. It is enough to add one extra term: $\overline{A_1'A_1}$.

$$\langle A_1A_2\rangle + \langle A_2A_3\rangle + \langle A_3A_4\rangle + \langle A_4A_5\rangle + \langle A_5A_1'\rangle - \overline{A_1'A_1} \geq -4. \tag{2.4}$$

The derivation of the modified inequality is analogous to that of the original KCBS inequality, with the function $K(a_i)$ replaced by $K'(a_i) = a_1a_2 + a_2a_3 + a_3a_4 + a_4a_5 + a_5a_1' - a_1'a_1$. Although, mathematically, the new inequality is very similar to the original one, physically, the last term is different from the others. Because the measurements for A_1 and A_1' occur at different stages of the experiment, the last term cannot be measured in the same way as the other ones. We must therefore be able to write the additional term $\overline{A_1'A_1}$ in terms of quantities that are experimentally accessible. Whenever $A_1' = A_1$ the sixth term is equal to $+1$, otherwise it equals -1, giving

$$\overline{A_1'A_1} = P(A_1 = A_1') - P(A_1 \neq A_1'). \tag{2.5}$$

The problem, now, reduces to finding experimentally when the two measurements have the same result, and when not. Physically this can be viewed as checking how well the mode $|\vec{l_1}\rangle$ is mapped onto the mode $|\vec{l_1'}\rangle$. If the mapping was perfect i.e. if $|\vec{l_1}\rangle = |\vec{l_1'}\rangle$, the two measurements would be identical and have always the same results. This would mean that whenever we block one of the modes the other one is blocked as well. We base our method of measurement of $\overline{A_1'A_1}$ on this observation.

We can expand the two probabilities from equation 2.5 using conditional ones:

$$\begin{aligned} P(A_1 = A_1') &= P(A_1' = +1|A_1 = +1)P(A_1 = +1) + \\ &\quad P(A_1' = -1|A_1 = -1)P(A_1 = -1), \end{aligned} \tag{2.6}$$

$$\begin{aligned} P(A_1 \neq A_1') &= P(A_1' = -1|A_1 = +1)P(A_1 = +1) + \\ &\quad P(A_1' = +1|A_1 = -1)P(A_1 = -1). \end{aligned} \tag{2.7}$$

Inserting 2.6 and 2.7 into 2.5 and using the normalization condition, we arrive at

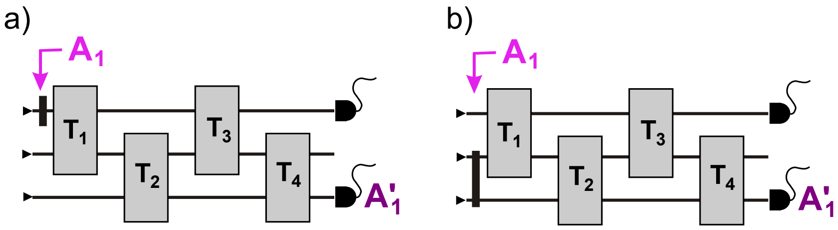

Figure 2.8: Conceptual scheme of the additional blocking stages for the measurement of $\epsilon = 1 - \overline{A_1'A_1}$. As in Fig. 2.5, straight, black lines represent optical modes (beams). Gray boxes represent transformations. Vertical black lines represent mode blocks, which absorb the photons in the mode(s) they are inserted into. If, with a block placed before the transformation T_1, a photon still reaches one of the detectors, we conclude that it did not hit the block (i.e., a detector positioned in place of the block would not have clicked). Thus, a) having a block in the uppermost mode allows us to measure the conditional probability $P(A_1' = -1|A_1 = 1)$, while b) blocking the two remaining modes allows us to measure $P(A_1' = 1|A_1 = -1)$.

$$\begin{aligned}\overline{A_1'A_1} = 1 - 2(&P(A_1' = -1|A_1 = +1)P(A_1 = +1) + \\ &P(A_1' = +1|A_1 = -1)P(A_1 = -1)).\end{aligned} \tag{2.8}$$

The four conditional probabilities $P(A_1' = \pm - 1|A_1 = \pm 1)$ can be accessed by blocking the appropriate modes at the stage of A_1 and monitoring the outcome at the final stage. For instance, $P(A_1' = 1|A_1 = -1)$ can be measured by blocking the modes that would give -1 at the stage of A_1 and registering the probability for A_1' to be assigned $+1$ (see Fig. 2.8). We showed that the inequality 2.4 is experimentally testable. It can be rewritten as

$$\langle A_1A_2\rangle + \langle A_2A_3\rangle + \langle A_3A_4\rangle + \langle A_4A_5\rangle + \langle A_5A_1'\rangle \geq -3 - \epsilon, \tag{2.9}$$

where $\epsilon = 1 - \overline{A_1'A_1}$.

2.6 Links between the theory and the experiment

Above we described how one can test the KCBS inequality with an optical setup. We translated the mathematics into the physical setup. We can now make more links between the theoretical results and the physical implementation.

Topology of the KCBS diagram

Interestingly, the KCBS diagram can be drawn by a single line which does not go twice through any of its vertices and comes back to the vertex it started from. Using the language of graph theory, we can say that the KCBS graph is Hamiltonian. Importantly for experimental implementation, the KCBS graph is Eulerian, i.e. there is a way of tracing it such that the trail goes through each edge exactly once (each edge represents a pair of measurements). This is exactly what is important for a BKS experiment, which requires measurements of all the commuting sets of observables from a given BKS diagram, because the number of steps should be as small as possible. Bigger three-dimensional BKS diagrams are not Eulerian and, as a consequence, an experiment would be less economical. In the cases analysed by Larsson, the number of rotations required to trace the diagram varied between 72 and 96 for various three-dimensional diagrams involving 31 and 33 vectors (table on p.7 [46]). In the case of the KCBS proof we need 4 rotations connecting 5 vectors.

Irregular pentagrams

From the theoretical description we know that regularity of the pentagram is not essential for the KCBS argument (see 1.3.3). The regular pentagram is optimal, but other pentagrams also provide a violation of the inequality. This is important for real experiments, because there we cannot expect the settings to be perfect, so even if we aim for a regular pentagram, we will obtain a distorted one. Fortunately, this does not affect our argument, but only decreases the maximal possible violation of the KCBS inequality.

Edges – compatible measurements

It is important that a diagram is indeed realised. This means that the vertices need to be connected – pairs of measurements must indeed commute. In our case they commute automatically. The measurements that we execute check if there is a photon in a given mode. Measurements commute when their corresponding modes are orthogonal, as they do not affect each other. Thus the commutativity requirement for pairs of comeasured observables is met naturally in our implementation.

Vertices – the same measurement in two contexts

The other property defining the diagram is the overlap of two lines at vertices. This means physically that there is one measurement common to two neighbouring pairs of measurements in the KCBS inequality (e.g. the same physical realisation of the measurement A_2 appears in the measurements of pairs $\langle A_1 A_2\rangle$ and $\langle A_2 A_3\rangle$). As we discussed above, this requirement is also met by our experiment naturally, because we keep one of the modes (and therefore the corresponding projector) untouched when moving between each pair of terms of the KCBS inequality.

Preparation - input state

Imperfect realisation of the transformations (rotations), apart from distortion of the pentagram, results in a misalignment of the input state with respect to the pentagram. This does not affect our argument. An imperfect input state only reduces the achievable violation.

Chapter 3

Physical realisation of the experiment

In this chapter we will describe the experimental setup that we used to test the KCBS inequality. We include the technical lessons we learnt when building the setup. We also explain how the design was found.

In the section 3.1 we describe how we generated single photons for the experiment. In the section 3.2 we explain how we obtained the physical design starting from the conceptual scheme. We present the relation between the two and give the mathematical description of the physical setup. We move on to technical aspects of the experiment (3.3) where we discuss the type of wave plates that we used, the way we constructed our setup and the prescription for finding the required orientations of the wave plates. At the end of the chapter we present the mathematical description of the setup.

3.1 Heralded single photon generation and detection

Since, in order to realise the scheme described in the previous chapter, we need to detect not only clicks, but also no-click events, we need to prepare the photons such that we know when they are supposed to reach the detectors. On-demand single photon source would be sufficient, but even a simpler to realise heralded photon source meets the requirements of the experiment. In such a source the time when a photon is generated is random, but once such event takes place we are notified by a herald. We use a very well developed and popular scheme of generation of heralded single photons by the process of spontaneous parametric down-conversion (SPDC) in a non-linear crystal. In this process, one pumps a crystal with non-zero second-order non-linearity with a laser. Pairs of photons which energies sum up to the energy of a pump photon are generated. Since in this process the photons are always generated in pairs, one can realise the heralding naturally. Detection of a photon, heralds the presence of its "brother" created in the same process.

We used a $20mm$ long, periodically poled Potassium Titanyl Phosphate (ppKTP) crystal in a type-II collinear process. In parametric down-conversion of type-II the two generated photons have orthogonal polarisations. Each of them is emitted onto a cone. Opening angles of the cones depend on the orientation of the crystal. Collinear phase-matching means that the two cones intersect along one line only. Radiation emitted along this line is used in the experiment. Traditional (angle) phase-matching is adjusted by tilting the crystal, for periodically poled crystal the phase-matching (called quasi-phase-matching) is changed by adjusting the temperature of the crystal.

In our experiment the temperature of the crystal was set to about $42°$ by a home-built Peltier oven to maximize the coincidence counts. We pumped the crystal with about $3mW$ of power from a grating-stabilized diode laser at about $405nm$ and collected the generated pairs of photons to single-mode fibres for spatial filtering. We obtained the rough alignment of the coupler by connecting a red diode laser to the single mode fibre and shining back through two irises centred at the pump beam. If care is taken, such alignment results already in some photon pairs coupled to the single mode fibre. We registered coincidences after a fibre 50/50 beam-splitter (such arrangement reduces the number of registered coincidences by a factor of two).

The diode laser that we used as a pump for the source was characterized by a transverse profile which was very far from the one of a single mode fibre mode, which in turn can be well approximated by a Gaussian beam. The profile was highly elliptical and had many local maxima (see Fig. 3.1). We noticed that introducing an iris and closing it partially till the transmitted power was about 10% of the total power did not diminish the coincidence counts. It follows that about $3mW$ of laser power was used for pumping the down-conversion. Fortunately, we did not need high power of the pump. Periodically poled crystals are very efficient and our experiment did not require high count rates. High count rates could even cause problems in this experiment (see 4.2.2). The ellipticity of the pump beam was taken care of by a pair of cyllindrical lenses. At the same time they were used to focus the beam into the nonlinear crystal.

After the crystal we needed to separate the down-converted photon pairs from the strong pump radiation. The process of down-conversion is very inefficient, so the pump radiation has many orders of magnitude bigger power than the SPDC. We used dichroic mirrors which were highly transmitive at the pump wavelength ($405nm$) and highly reflective at the wavelength at

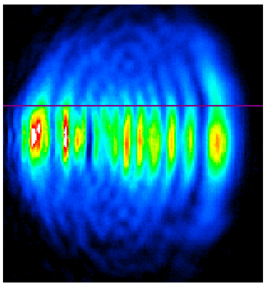

Figure 3.1: Transverse intensity profile of the output from a diode laser which after being transmitted through an iris and cylindrical lenses was used as a pump beam.

which the photon pairs are generated (around 810nm). Two of them followed by an interference filter (12nm FWHM; Andover 9500) and a long-pass filter was sufficient to suppress the pump radiation and reduce the noise. At the same time the dichroic mirrors were used to couple the down-converted radiation into a single mode fibre (SMF).

Thanks to coupling the photons to a single mode fibre we could separately optimize the source and the rest of the setup. For the former we would connect the output of the source to the detectors, and for the latter we would connect a diode laser as an input for the measurement setup instead of the single photon input.

The combination of wavelengths (405nm and 810nm) was used for technical reasons. It stems from a compromise between availability of standard laser diodes (usually longer wavelengths) and efficiency of avalanche photodiodes in the near infrared.

For single photon detection we used home-built avalanche photodiode single-photon detectors and coincidence logic. The effective coincidence window (including the jitter of the detector) is about 2.3ns.

3.2 Simplification of the setup using polarisation

The concept of the experiment described in Chapter 2 requires an experimental setup which is a complex three-way Mach-Zehnder interferometer with removable or tunable beam-splitters (see Fig. 2.5). Such setup if built in a straightforward way would be neither stable nor handy. We simplified the design by combining two of the modes into a single spatial mode carrying two polarisations (see Fig. 3.3).

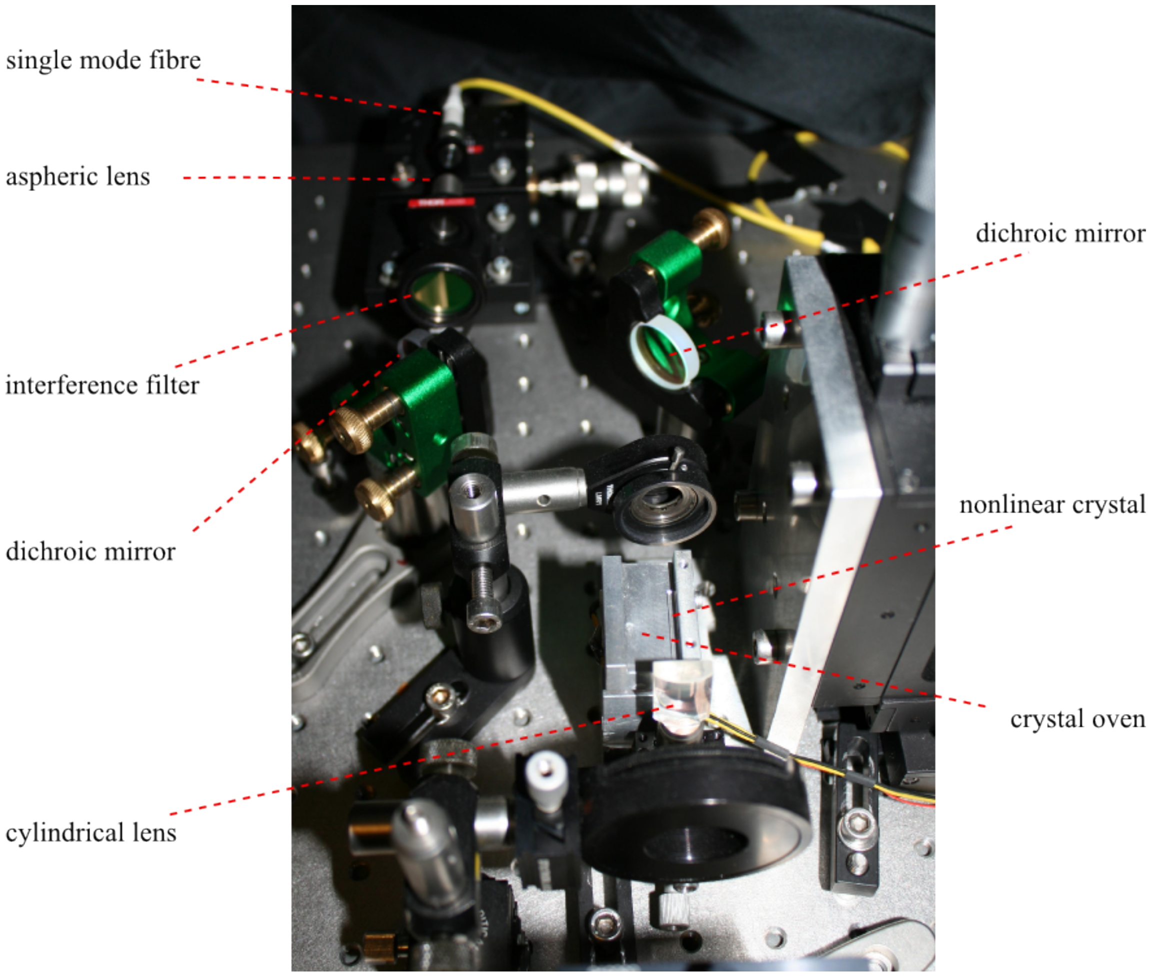

Figure 3.2: A photograph of the heralded single photon source. About $3mW$ of power from a grating-stabilized diode laser at $405nm$ is used to pump the nonlinear crystal ($20mm$ long, periodically poled Potassium Titanyl Phosphate – ppKTP) producing pairs of orthogonally polarised photons via spontaneous parametric down-conversion. The pump is filtered out with the help of a combination of dichroic mirrors and interference filters.

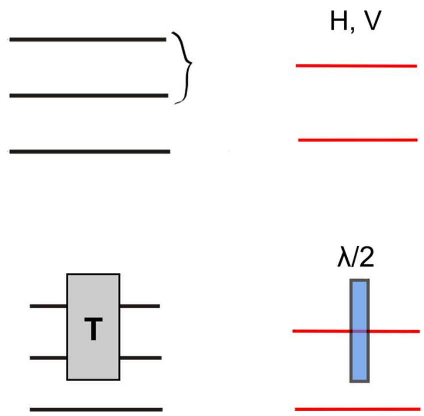

Figure 3.3: Simplification of the setup: three spatial modes are replaced by two spatial modes, one of which carries two polarisations (H – horizontal, V – vertical). The tunable beam-splitter (T) is replaced by a half-wave plate ($\lambda/2$).

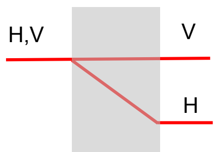

Figure 3.4: Calcite crystal used as a polarising beam splitter (PBS). Horizontal (vertical) polarization propagates as an extraordinary (ordinary) ray. Translation of the crystal does not affect the transmitted beams, which is crucial for the stability of the setup built from such crystals.

The transformations on the pairs of modes are conveniently performed by half-wave plates. As we need to apply the transformations to any pair of modes (see Fig. 2.5 in the Chapter 2), we rearrange the modes with the help of half-wave plates and blocks of calcite acting as polarising beam splitters (see Fig. 3.4). We keep only two spatial modes, until the polarisations are split for detection.

The crucial requirement of the experiment, that each transformation acts only on two modes and leaves the remaining one untouched, is met because each wave plate is inserted only into one beam and acts only on the two polarisation modes in this beam. It follows that there are common measurements in the adjacent pairs of measurements from the KCBS diagram. We obtained the design of our setup by translating the conceptual scheme from Fig. 2.5, i.e. by replacing each transformation by a half-wave plate, and splitting and combining the modes with the help of calcite PBSs. To do this, we had to introduce additional half-wave plates in the places were polarisation needed to be switched, their optical axes were set to 45° (all the orientations of polarisation elements are defined with respect to the horizontal axis defined by the orientation of the first PBS in the setup).

3.3 Construction of the setup and alignment procedure

In the section below we describe the technical details of the experiment.

3.3.1 Technical aspects of Mach-Zehnder interferometers based on polarising beam displacers

The experimental setup comprises three distinct Mach-Zehnder interferometers (see Fig. 3.8). We used them to construct and later diagnose the setup. Visibility of interference is given by

$$V = \frac{I_{max} - I_{min}}{I_{max} + I_{min}}, \tag{3.1}$$

where I_{max}/I_{min} denote the maximal/minimal intensity (maximum and minimum are found by varying the phase between the interfering modes). Visibility can be used to evaluate the quality of an interferometer. Deviation of the observed visibility from the maximal value of 1 is a measure of experimental imperfections. Owing to the use of single mode fibres at the input of the measurement setup we could test the interferometers independently from

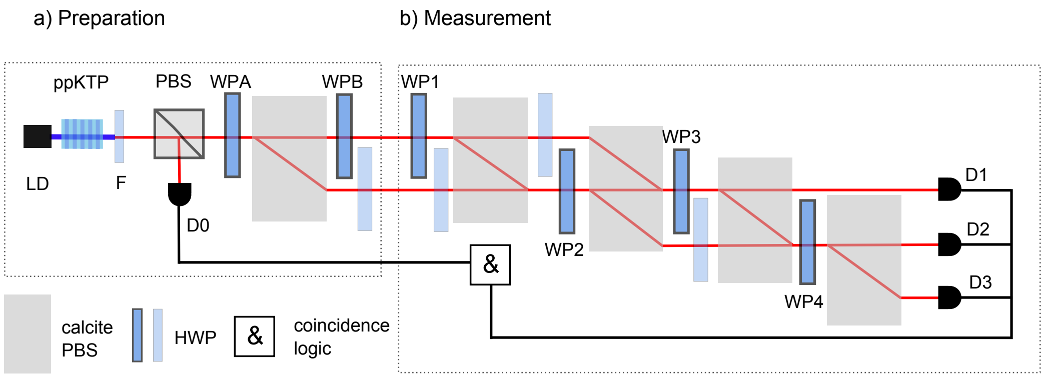

Figure 3.5: Experimental setup [12]. a) Preparation of the required single-photon state. About $3mW$ of power from a grating-stabilized diode laser at $405nm$ (LD) is used to pump the nonlinear crystal ($20mm$ long, periodically poled Potassium Titanyl Phosphate – ppKTP) producing pairs of orthogonally polarised photons via spontaneous parametric down-conversion. The pump is filtered out with the help of a combination of dichroic mirrors and interference filters (labeled jointly as F). The photon pairs are split at a polarising beam splitter (PBS). Detecting the reflected photon heralds the transmitted one. Half-wave plates WP_A and WP_B transform the transmitted photon into the desired three-mode state. Calcite polarising beam splitters separate and combine orthogonally polarised modes. In the measurement apparatus b) half-wave plates $WP_1 - WP_4$ realize the transformations $T_1 - T_4$ on pairs of modes. Each transformation can be "turned off" by setting the optical axis of the corresponding wave plate vertically (at 0°). The unlabeled (light blue) wave plates serve to balance the path lengths and to switch between horizontal and vertical polarization (the second unlabelled wave plate is set to 0°, the rest is set to 45°). Detecting heralded single photons means in practice registering coincidences between single photon detectors: D_0 and each of D_1, D_2, and D_3. Registrations in two of the detectors D_1, D_2, and D_3 give the values A_i necessary for the inequality (see Fig. 4.1). The third detector is used to identify the trials when the photon is lost. Note that the assignment of measurements to detectors in the experimental setup differs in some cases from that described in the simplified conceptual scheme (Fig. 2.5). We use home-built avalanche photodiode single-photon detectors and coincidence logic. The effective coincidence window (including the jitter of the detector) is about $2.3ns$.

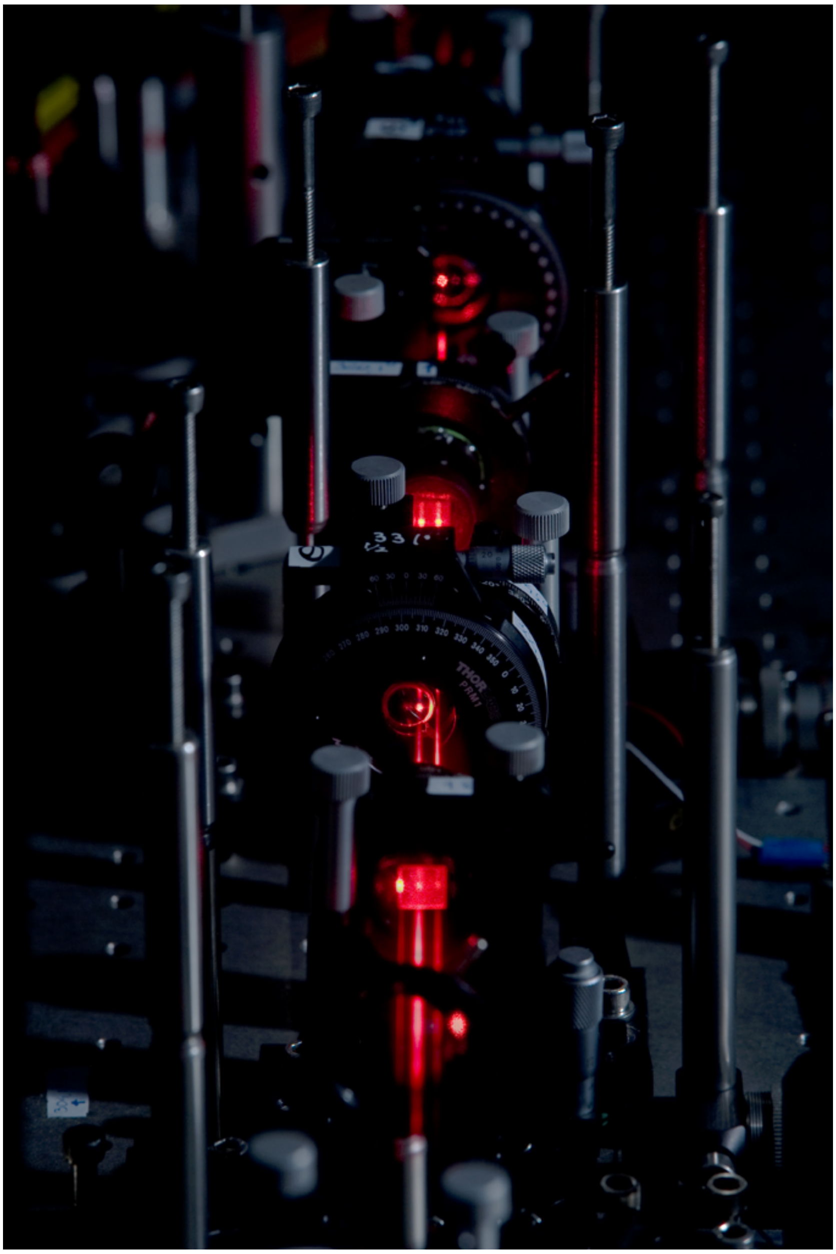

Figure 3.6: A photograph of the central part of the measurement setup. The elements with square apertures are the calcite PBSs and the round ones are half-wave plates. One can see a beam passing through a wave plate and the other one passing next to it. We made the beams visible by connecting a red diode laser to the output of the setup (where normally the photon-detecotrs were connected) and making the laser light scatter at a vapour created with liquid nitrogen. Please note, that this photograph is not intended to faithfully document the experiment, but to show the main parts of the experimental setup. The wavelength and polarisation of the laser diode were different than those of the photons used in the experiment, which results in different positions of the beams.(Copyright: IQOQI; J. Godany 2011).

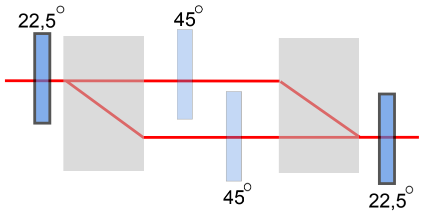

Figure 3.7: Mach-Zehnder interferometer based on calcite polarizing beam splitters. Blue rectangles represent half-wave plates (their orientations are given in the figure).

the single photon input state.

For visibility measurements we set the orientations of half-wave plates such that we obtained a Mach-Zehnder interferometer with balanced beam splitters (see Fig. 3.7). The outer wave plates were set to 22.5° and the wave plates between the calcite crystals were set to 45°. We performed the tests with a home-built grating stabilized diode laser, which made them both easier and more reliable then the measurements with single photons. We measured the visibility of each of the three interferometers and obtained the following values $V_{MZ1} \approx 99.8\%$,$V_{MZ2} = 99.6\%$, $V_{MZ3} \approx 99\%$ for a single half-wave plate acting at two beams set to 45°. Those values lowered slightly when the single wave plate was replaced by two separate wave plates (see Fig. 3.8). We used a CCD camera to check if the spatial mode is not distorted by wave plates that we introduced into the setup. Fast photodiodes served us to record interference fringes. For the measurements of visibility we used power meters.

Stability

The interferometer based on polarising beam displacers is very stable. One of the reasons for the outstanding stability is that with such a design the interferometer is not sensitive to translations of the optical components (this is not the case for the standard Mach-Zehnder interferometer). The beam displacers can be translated without affecting the beams. Only tilts change the optical phase (this was the way we used to set the phase in the experiment).

Calibration of polarisation sensitive components

Most of the relevant components of our setup act on polarisation. They needed to be calibrated using a single reference element to ensure proper

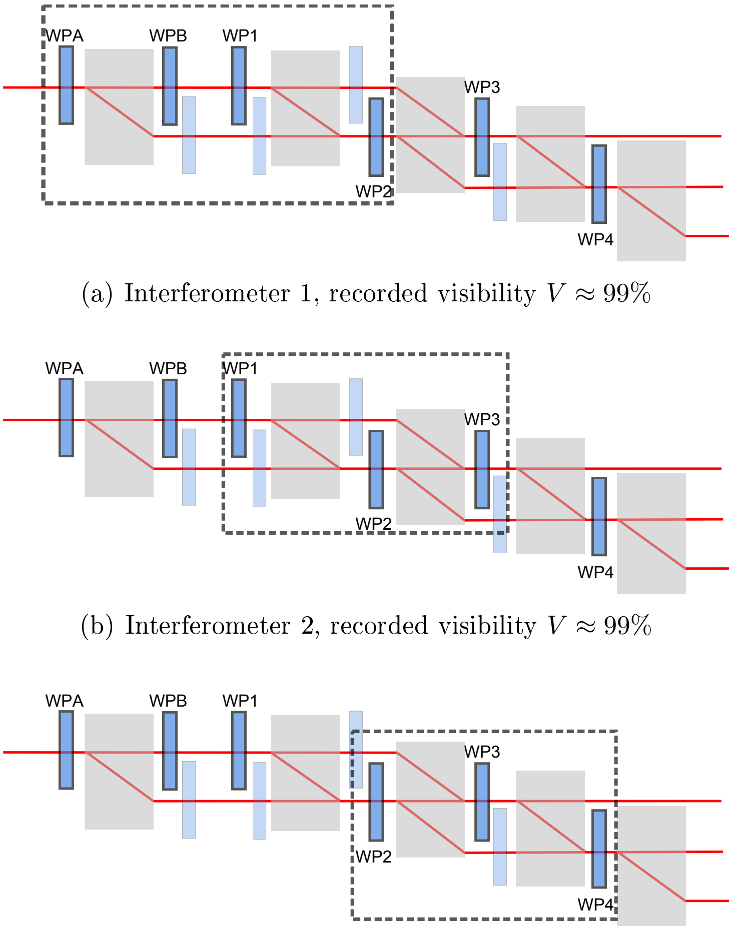

(a) Interferometer 1, recorded visibility $V \approx 99\%$

(b) Interferometer 2, recorded visibility $V \approx 99\%$

(c) Interferometer 3, recorded visibility $V \approx 98.6\%$

Figure 3.8: Three Mach-Zehnder interferometers within the experimental setup marked by dashed boxes. The wave plates in each interferometer were set as in Fig. 3.7. The values of visibilities were measured with wave plates acting on single beams inside the interferometer.

alignment and correct measurement settings. We used a polarisation beam splitter (PBS) at which the signal and idler photons are split to define the horizontal polarisation for our experiment. We used calcite beam displacers (BD40, Thorlabs; $10 \times 10 \times 40mm^3$) as polarizing beam splitters. We calibrated them with the help of the first PBS. When calibrating, we were adding the optical components one by one, i.e. we were calibrating each element in situ (see Fig. 3.9).

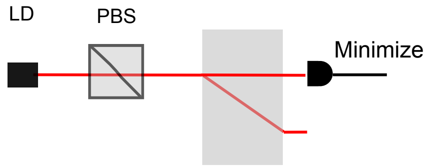

(a) Setting the orientation of the first calcite polarising beam splitter with the help of a cube PBS. Recorded contrast $C \approx 2 \cdot 10^3$.

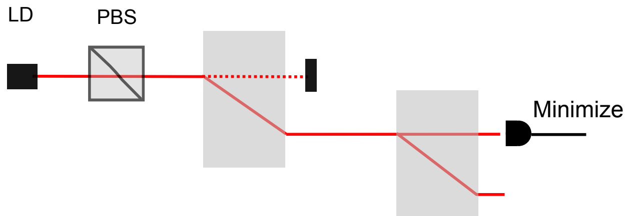

(b) Setting the orientation of the second calcite polarising beam splitter with the help of the first one. Recorded contrast $C \approx 5 \cdot 10^4$

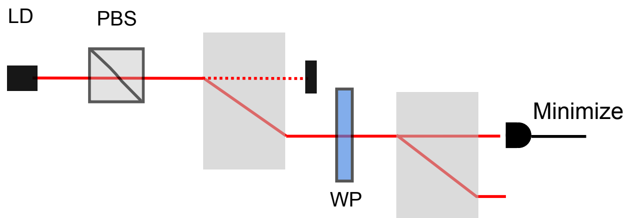

(c) Setting the orientation of a half-wave plate using two calcite polarising beam splitters acting as "crossed polarisers". Recorded contrast $C \approx 1.5 \cdot 10^3$

Figure 3.9: Parts of the setup used for calibration of polarisation elements. LD - diode laser, PBS - polarising beam splitter, WP - half-wave plate, grey rectangles denote calcite polarising beam splitters. We used the contrast $C = \frac{I_{max}}{I_{min}}$ to evaluate the quality of the polarisation elements.

Alignment procedure

The alignment procedure of interferometers based on polarising beam displacers is different than that of standard Mach-Zehnder interferometers. One does not need to adjust the spatial overlap of the two interfering beams. If the calcite crystals have the same length and cut angle, orienting them in the same way ensures the spatial overlap of the two interfering beams. Setting the orientation in the plane orthogonal to the direction of propagation of the ordinary ray can be done very precisely with the help of polarisation – by minimizing the intensity at the output of the "crossed" polarisers . The tilt in horizontal and vertical directions can be eliminated with the help of the laser light reflected from the facets of the calcite crystals – we directed the beam from a red alignment laser back to the coupler. In the last stage of alignment we needed to assure that the path difference between the two interferometer arms is smaller than the coherence length of the down-converted photons. Scanning the interference fringes using down-conversion would be inconvenient, because of the low count rates and the resulting low speed of scanning. We used a multimode laser diode. We observed the output of the interferometer with a fast photodiode connected to an oscilloscope, while scanning the fringes by tilting one of the crystals. We used a tiltable stage equipped with a differential micrometer screw.

As can be seen at the Fig. 3.5 one of the polarising beam displacers has to transmit three beams. The beams are separated by about $4mm$, and the crystal has a clear aperture of $10 \times 10mm^2$, so in order to avoid clipping the beams at the edges of the crystal, the beam needs to be focused at the central crystal and the crystal itself needs to be positioned and oriented very carefully. This makes this crystal the most sensitive part of the setup. We mounted it on a horizontal translation stage (orthogonal to the direction of the beams) that allowed us to find the optimal position.

For out-coupling and collection of photons we used microscope objectives with magnification of $10\times$. We collected the photons to multimode fibers (graded index, $62.5\mu m$ core diameter). We did not need to define the modes with the single mode fibers at the end of the setup, because they were defined by a single mode fiber already at the beginning of the measurement part of the setup, just after the photon source.

3.3.2 Design of the wave plates

Wave plates that we used had to affect only one of the two spatial modes. The distance between the centres of the two beams was determined by the length of the calcite crystal and the walk-off angle of calcite, it was approximately $4mm$. The distance is too small for wave plates mounted in a standard way to act on one beam only. Longer crystals are expensive and are not available as standard products. We ordered 1/2 inch diameter wave plates mounted on 1 inch diameter BK7 glass plates and let one of the beams pass through the glass and the other through the wave plate and glass (custom product from Foctek). We noticed that placing a wave plate in an interferometer reduced the observed interference visibility substantially (down to $80\% - 90\%$). We tested the wave plates separately with the help of a laser diode and a

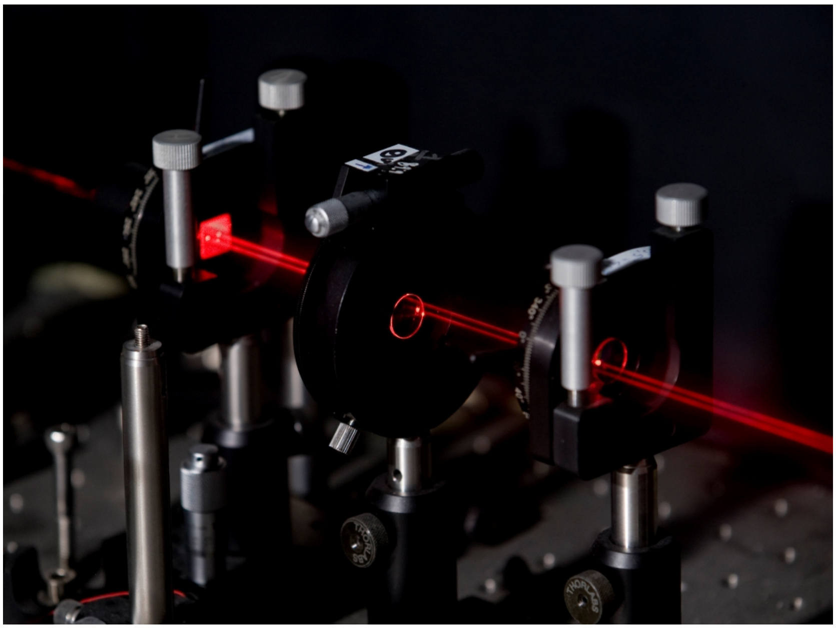

Figure 3.10: Part of the experimental setup. From the left: calcite PBS, two half-wave plates. One beam passing through a wave plate and the other one passing next to it. We made the beams visible by connecting a red diode laser to the input of the setup (where normally the photon-source was connected) and making the laser light scatter at vapour created with liquid nitrogen. A red ($\lambda = 670nm$) laser diode was used, which results in slightly different positions of the beams than for the infrared radiation. (Copyright: IQOQI; J. Godany 2011).

camera and noticed that they not only displace the transmitted beam but also change its direction, which is detrimental to the interference visibility. This means that the faces of the wave plate are not parallel to the facets of the glass plate the wave plate was cemented onto. The cement layer is a wedge which bends the transmitted light. To solve the problem of wave plates without ordering extra custom products we decided to use bare 1/2 inch wave plates mounted such, that there is space next to them for a second beam. We took the standard Thorlabs wave plates out of their housing, cut the housing into four parts and glued the wave plate to one of the parts. We could use a standard rotation mount to hold such wave plate. Suprisingly, although the wave plate's surface was not orthogonal to the beam passing through it, it did not diminish the interference visibility drastically ($98.5\% - 99.5\%$). To balance the dispersion in the two arms of each interferometer we placed additional wave plates which were set either to $0°$ or to $45°$.

3.3.3 Orientations of the wave plates

The calibration of wave plates was performed modulo $90°$. Rotation of a wave plate by $\pm 90°$ corresponds to swapping its fast and slow axes. This transformation only results in a phase-shift that the beam with the wave plate acquires relative to the other beam. This phase-shift is compensated automatically in our experimental procedure where we adjust the overall phase differences in the Mach-Zehnder interferometers.

3.3.4 Introducing phase-shifts and finding the "zero-delay"

In the first versions of the experimental setup we were introducing the phase in the interferometers by a combination of wave plates resulting in geometric phase. At the input of the polarisation Mach-Zehnder interferometer we placed a pair of quarter-wave plates at $45°$ with a half-wave plate between them. The rotation of the half-wave plate by angle α results in a change of phase between the two polarisations by 4α.

The advantage of the combination of quarter-, half-, and quarter-wave plates is the precision and repeatability. Unfortunately it requires three additional optical elements for each phase-shift. Each wave plate is imperfect both in the delay it introduces between the polarisations and in the orientation. On top of this, wave plates, as all optical elements introduce losses, wavefront distortions, shifts and tilts of the transmitted beam. All the above

Measured quantity	WP_A/ °	WP_B/ °	WP_1/ °	WP_2/ °	WP_3/ °	WP_4/ °	Polarizer
$\langle A_1 A_2 \rangle$	-24.0	-58.0	0.0	0.0	0.0	0.0	-
$\langle A_2 A_3 \rangle$	-24.0	-58.0	109.1	0.0	0.0	0.0	-
$\langle A_3 A_4 \rangle$	-24.0	-58.0	109.1	109.1	0.0	0.0	-
$\langle A_4 A_5 \rangle$	-24.0	-58.0	109.1	109.1	109.1	0.0	-
$\langle A_5 A_{1'} \rangle$	-24.0	-58.0	109.1	109.1	109.1	-64.1	-
$P(A_{1'} = -1 \mid A_1 = 1)$	-24.0	-58.0	109.1	109.1	109.1	-64.1	0.0
$P(A_{1'} = 1 \mid A_1 = -1)$	-24.0	-58.0	109.1	109.1	109.1	-64.1	90.0

Figure 3.11: Orientations of all the relevant half-wave plates at various stages of the experiment. Only one half-wave plate at a time changes orientation when we change the term of the inequality that is measured.

effects are detrimental for the interference visibility. We observed a drop in visibility when introducing the quarter-, half-, quarter-wave plate combination before the interferometer. We turned to a simpler method of introducing the phase, which did not require any additional components and allowed us to introduce also optical delays necessary to maximize the interference visibility.

We were introducing the phase in the interferometers, by tilting the calcite crystals. To obtain the maximal visibility of interference it was crucial to find the "central fringe" – zero delay between the two arms of the interferometer. We scanned the interference fringes obtained with a multimode diode laser. The coherence length of the diode was low enough for the variation of the contrast to be visible when scanning the fringes on a sub-millimetre scale. This allowed us to find the fringe with the highest contrast where all the modes of the laser were in phase.

The phases of the interferometers need to be set to zero in order for the setup to realize the geometry of the KCBS proposal (all the coefficients involved are real). However the errors in the phase setting, as well as the errors in the orientations of wave plates, do not affect the argument. Instead they result in smaller violation of the KCBS inequality (see 1.3.3). We set the phase in the interferometers with the help of a diode laser. While tuning the phase, by tilting the calcite beam-displacers, we were minimizing the intensity in appropriate modes.

3.4 Mathematical description of the optical setup

In the previous chapter we discussed the geometry of the KCBS proposal. We described the transformations involved as rotations in a three-dimensional real space, however the transformation performed by a half-wave plate is not a rotation. We will show below that it is a reflection with the axis of reflection being the optical axis of the wave plate. Such an operation also allows us to transform one basis into another. In the present section we describe the obtained setup mathematically and show that it indeed realises the KCBS measurements.

3.4.1 Rotations in a three-dimensional real space

Let us start by writing down matrices representing two-dimensional rotations in three-dimensional space. A rotation about the x-axis by angle α is represented by a matrix:

$$R_x(\alpha) = \begin{pmatrix} 1 & 0 & 0 \\ 0 & \cos\alpha & -\sin\alpha \\ 0 & \sin\alpha & \cos\alpha \end{pmatrix}. \tag{3.2}$$

A rotation about the y-axis is given by:

$$R_y(\alpha) = \begin{pmatrix} \cos\alpha & 0 & -\sin\alpha \\ 0 & 1 & 0 \\ \sin\alpha & 0 & \cos\alpha \end{pmatrix}, \tag{3.3}$$

and a rotation about the the z-axis:

$$R_z(\alpha) = \begin{pmatrix} \cos\alpha & -\sin\alpha & 0 \\ \sin\alpha & \cos\alpha & 0 \\ 0 & 0 & 1 \end{pmatrix}. \tag{3.4}$$

where each rotation keeps one of the below basis vectors fixed:

$$\hat{x} = \begin{pmatrix} 1 \\ 0 \\ 0 \end{pmatrix}, \hat{y} = \begin{pmatrix} 0 \\ 1 \\ 0 \end{pmatrix}, \hat{z} = \begin{pmatrix} 0 \\ 0 \\ 1 \end{pmatrix}. \tag{3.5}$$

3.4.2 Jones matrix of a half-wave plate

We will compare the action of a half-wave plate with a rotation. We will start by finding the Jones matrix of a half-wave plate. A wave plate introduces a phase difference δ between the components polarised along and perpendicular to its fast axis (physically this can be realised with the help of birefringence):

$$W_\delta = \begin{pmatrix} 1 & 0 \\ 0 & e^{i\delta} \end{pmatrix}. \tag{3.6}$$

For a half-wave plate the delay between the polarisations $\delta = \pi$ (this is where its name comes from).

$$W \equiv W_{\lambda/2} = \begin{pmatrix} 1 & 0 \\ 0 & -1 \end{pmatrix}. \tag{3.7}$$

Note that W is a matrix of reflection.

The orientation of the fast axis can be set by rotating the half-wave plate. To describe a wave plate rotated with respect to the coordinate system of the experiment we need to use the following product of matrices:

$$W(\alpha) = R_{-\alpha} W_{\lambda/2} R_\alpha = \begin{pmatrix} \cos(2\alpha) & -\sin(2\alpha) \\ -\sin(2\alpha) & -\cos(2\alpha) \end{pmatrix}, \tag{3.8}$$

where R_α is matrix representing a rotation by α (see 2.2). We see that a half-wave plate matrix $W(\alpha)$ is similar to a rotation matrix, but its determinant equals -1 whereas it is $+1$ for rotation matrices. However, what matters for the BKS argument is to perform transformations between given coordinate systems. Note that, unlike for rotations for which $R(0) = I$ (I denotes the identity matrix), wave plates set to $0°$ should be taken into account in the calculations, because $W(0) \neq I$.

3.4.3 Wave plates acting in a three-mode space

We have three modes in an interferometric setup so the matrices describing the setup should be three-dimensional. This will allow us to keep track of phases introduced in Mach-Zehnder interferometers and by wave plates.

The main building blocks of the setup are wave plates. Therefore we explicitly write down the matrices of wave plates acting on one spatial mode only:

$$W_{12}(\alpha) = \begin{pmatrix} \cos(2\alpha) & -\sin(2\alpha) & 0 \\ -\sin(2\alpha) & -\cos(2\alpha) & 0 \\ 0 & 0 & 1 \end{pmatrix}, \tag{3.9}$$

$$W_{13}(\alpha) = \begin{pmatrix} \cos(2\alpha) & 0 & -\sin(2\alpha) \\ 0 & 1 & 0 \\ -\sin(2\alpha) & 0 & -\cos(2\alpha) \end{pmatrix}, \tag{3.10}$$

$$W_{23}(\alpha) = \begin{pmatrix} 1 & 0 & 0 \\ 0 & \cos(2\alpha) & -\sin(2\alpha) \\ 0 & -\sin(2\alpha) & -\cos(2\alpha) \end{pmatrix}. \tag{3.11}$$

We described the transformations, now we need to define the vectors they act upon. As in Jones formalism we define the basis states as:

$$\vec{d_1} = \begin{pmatrix} 1 \\ 0 \\ 0 \end{pmatrix}, \vec{d_2} = \begin{pmatrix} 0 \\ 1 \\ 0 \end{pmatrix}, \vec{d_3} = \begin{pmatrix} 0 \\ 0 \\ 1 \end{pmatrix}. \tag{3.12}$$

We label the modes right before the detectors. If there was no wave plates, those modes would go back straight to the beginning of the setup.

3.4.4 Description of the entire setup: combining the transformations

We will apply wave plate transformations to the modes while propagating back from the detectors to the beginning of the setup. In this way we learn what is the mode that the detector "sees".

Wave plates transform the modes $(\vec{d_1}, \vec{d_2}, \vec{d_3})$ to $(\vec{l_1}, \vec{l_2}, \vec{l_{\overline{12}}})$, $(\vec{l_2}, \vec{l_3}, \vec{l_{\overline{23}}})$,..., or $(\vec{l_5}, \vec{l_1}, \vec{l_{\overline{51}}})$ depending on their settings. $\vec{l_i}$ are the vectors (modes) constituting the KCBS pentagram and $\vec{l_{ij}} = \vec{l_i} \times \vec{l_j}$ are the vectors completing each basis, which are not explicitly involved in the proof. To trace back which of the three modes $\vec{d_i}$ is transformed onto given $\vec{l_i}$, we used the inverse of the total transformation performed by the combination of all the wave plates. Since for the wave plates $W^{-1} = W$, the inverse corresponds to reversing the order of applied transformations.

Below we give the product of all the transformations for the five modes involved in the experiment – corresponding to the five directions at the KCBS diagram. We include the phases of the interferometers.

$$
\begin{aligned}
\vec{l_1} &= W_{13}(\alpha_1)\Phi_1 W_{23}(\alpha_2)\vec{d_2}, \\
\vec{l_2} &= W_{13}(\alpha_1)\vec{d_1}, \\
\vec{l_3} &= W_{13}(\alpha_1)\Phi_1 W_{23}(\alpha_2) W_{23}(\alpha_3)\vec{d_3}, \\
\vec{l_4} &= -W_{13}(\alpha_1)\Phi_1 W_{23}(\alpha_2) W_{23}(\alpha_3) W_{12}(\alpha_4)\ \vec{d_2}, \\
\vec{l_5} &= -W_{13}(\alpha_1)\Phi_1 W_{23}(\alpha_2) W_{23}(\alpha_3) W_{12}(\alpha_4)\ \Phi_3 W_{13}(\alpha_5)\vec{d_1}, \\
\vec{l'_1} &= -W_{13}(\alpha_1)\Phi_1 W_{23}(\alpha_2) W_{23}(\alpha_3) W_{12}(\alpha_4)\ W_{13}(0) W_{13}(\alpha_5)\Phi_3\Phi_2(\alpha_6)\vec{d_2},
\end{aligned}
\tag{3.13}
$$

where Φ_1, Φ_2, Φ_3 are the following matrices describing π phase shifts in the Mach-Zehnder interferometers(MZ1, MZ3, MZ2, respectively) :

$$
\Phi_1 = \begin{pmatrix} -1 & 0 & 0 \\ 0 & 1 & 0 \\ 0 & 0 & 1 \end{pmatrix}, \tag{3.14}
$$

$$
\Phi_2 = \begin{pmatrix} 1 & 0 & 0 \\ 0 & -1 & 0 \\ 0 & 0 & 1 \end{pmatrix}, \tag{3.15}
$$

$$
\Phi_3 = \begin{pmatrix} 1 & 0 & 0 \\ 0 & 1 & 0 \\ 0 & 0 & -1 \end{pmatrix}. \tag{3.16}
$$

α_i $(i \in \{1, 2, ..., 6\})$ denote the orientations of the wave plates:

$$
\begin{aligned}
\alpha_1 &= -24^\circ, \\
\alpha_2 &= -58^\circ, \\
\alpha_3 &= 109.1^\circ, \\
\alpha_4 &= 109.1^\circ, \\
\alpha_5 &= 109.1^\circ, \\
\alpha_6 &= -64.1^\circ.
\end{aligned}
\tag{3.17}
$$

Chapter 4

Experimental results

Using the setup described in the previous chapter we tested the KCBS inequality and obtained $-3.893(6)$ for its left-hand side, which lies 120 standard deviations below the classical bound of $-3.081(2)$. In this chapter we describe how we used the setup to acquire the data (section 4.1) and how we processed the data to obtain the final result i.e. the value of the left hand side of the KCBS inequality and the experimental uncertainty (Eq. 4.2). We also discuss the systematic effects and how we deal with them. This includes relative efficiencies estimation, errors in the orientation of wave plates, double heralded clicks and phase drifts.

4.1 Experimental procedure and results

Although the interferometer based on calcite polarising beam splitters is passively stable, there is always some residual instabilities due to mechanical vibrations, air flows, and temperature drifts. To minimize the effect of instabilities, we tried to perform the experiment as fast as possible. First, we were moving from the measurement $\langle A_1 A_2 \rangle$ to the measurement of $\langle A_5 A_1' \rangle$. We were setting the phases in all three Mach-Zehnder interferometers (see Fig. 3.8) and orientations of the transformation wave plates ($WP_1 - WP_4$). In this direction we were using a diode laser ($\lambda \approx 810nm$) and power meters to set the phases.

When going in the opposite direction we were setting the orientations of the wave plates to $0°$, such that they do not affect the polarisation of the transmitted light. In five steps we went from $\langle A_5 A_1' \rangle$ to $\langle A_1 A_2 \rangle$. At each step, we recorded photons for $1s$, registering about 3500 heralded single photons. We repeated each stage 20 times, averaged the results, and calculated the standard deviation of the mean to estimate the standard uncertainties, which we then propagated to the final results (see Fig. 4.1), using the standard small error propagation rules.

From our measurements, we compute ϵ, the term quantifying the mismatch between A_1 and A_1':

$$\epsilon = 0.081(2), \tag{4.1}$$

thus bounding the left-hand side of the KCBS inequality (2.9) by $-3.081(2)$. Each of the terms on the left-hand side of the inequality takes a value of less than -0.7, adding to give:

$$\langle A_1 A_2 \rangle + \langle A_2 A_3 \rangle + \langle A_3 A_4 \rangle + \langle A_4 A_5 \rangle + \langle A_5 A_1' \rangle = -3.893(6). \tag{4.2}$$

This represents a violation of the KCBS inequality by more than 120 standard deviations, demonstrating that no joint probability distribution is capable of describing our results. The violation also excludes any non-contextual hidden variable model.

4.2 Systematic effects

In this section we describe the systematic effects present in the experiment. Those include inaccuracies in the orientation of half-wave plates and the settings of phase shifts, unequal losses of various paths through the setup and detection-related effects.

4.2.1 Unequal collection efficiencies

The count rates were corrected for differences in detector efficiencies and losses before the detectors. We obtained the correction factors, which we called single-output relative efficiencies, from the same series of measurements that we used to measure the values of the left-hand side of the KCBS inequality. Our method is based on the fact that ideally (if the three relative efficiencies are properly accounted for) the sum of the count rates at the three detectors does not depend on the settings of the apparatus (e.g. wave plate orientations). In such a case, only the distribution of counts rates among the detectors can change. Using this condition we could estimate the single-output efficiencies and calculate the corrected probabilities of detection according to:

D1		D2		D3		Calculated contribution	
condition	value	condition	value	condition	value	term	value
$P(A_1=1, A_2=-1)$	0.471(3)	$P(A_1=-1, A_2=1)$	0.432(3)	$P(A_1=1, A_2=1)$	0.097(1)	$\langle A_1A_2\rangle$	-0.805(2)
$P(A_2=-1, A_3=1)$	0.473(4)	$P(A_2=1, A_3=1)$	0.098(2)	$P(A_2=1, A_3=-1)$	0.429(4)	$\langle A_2A_3\rangle$	-0.804(3)
$P(A_3=1, A_4=1)$	0.146(2)	$P(A_3=1, A_4=-1)$	0.429(2)	$P(A_3=-1, A_4=1)$	0.426(2)	$\langle A_3A_4\rangle$	-0.709(3)
$P(A_4=1, A_5=-1)$	0.466(2)	$P(A_4=-1, A_5=1)$	0.439(2)	$P(A_4=1, A_5=1)$	0.095(1)	$\langle A_4A_5\rangle$	-0.810(2)
$P(A_5=-1, A'_1=1)$	0.469(2)	$P(A_5=1, A'_1=-1)$	0.414(2)	$P(A_5=1, A'_1=1)$	0.117(2)	$\langle A_5A'_1\rangle$	-0.766(3)
						Σ	**-3.893(6)**

D1	D3	D1 + D3		D2		Calculated contribution	
		condition	value	condition	value	term	value
0.788(2)	0.196(2)	$P(A'_1=1\|A_1=1)$	0.983(1)	$P(A'_1=-1\|A_1=1)$	0.017(1)	$-3-\varepsilon$	**-3.081(2)**
0.010(1)	0.062(2)	$P(A'_1=1\|A_1=-1)$	0.072(2)	$P(A'_1=-1\|A_1=-1)$	0.928(2)		

Figure 4.1: Collected experimental results. The value columns contain the measured probabilities corrected for relative efficiencies. Estimates of standard uncertainties (standard deviations of the means) are given in the brackets. The condition columns contain assigned measurement values (in label brackets) corresponding to heralded single-click events. Because of low detection efficiency, we need to use a third detector. It enables us to identify and discard trials in which a photon was lost (heralded no-click events). The rates of heralded double clicks (simultaneous responses of heralding detector and two other detectors) are negligible – typically two orders of magnitude smaller than the standard deviation in the rate of heralded single clicks. **Top:** Results for the KCBS inequality. Rows 1-5 correspond to terms 1-5 of inequality 1.13, and are measured with the corresponding devices illustrated in Figs 2.5.b-f. The last column is given by $\langle A_iA_j\rangle = P(A_i = 1, A_j = +1) - P(A_i = -1, A_j = +1) - P(A_i = +1, A_j = -1)$ **Bottom:** Extended bound. Rows 1 and 2 (corresponding to Figs 2.8a and 2.8b display the contributions to the conditional probabilities that are necessary to evaluate the additional terms in the extended KCBS inequality (2.9).

$$P(D_i) = \frac{\tilde{N}_i}{\sum_{j=1}^{3} \tilde{N}_j}, \tag{4.3}$$

where

$$\tilde{N}_i = \frac{N_i}{\eta_i} \tag{4.4}$$

is the measured number of heralded clicks at detector i ($i \in 1, 2, 3$) divided by the corresponding relative efficiency η_i. In our experiment, the main contribution to the differences in relative efficiencies comes from differing efficiencies of the detectors themselves.

4.2.2 Detection-related effects

Because of the low detection efficiency, we needed to use three detectors in the measurement apparatus. In cases when we recorded a heralding photon (detector D_0 at Fig. 3.5) and no photon in the measurement setup (detectors D_1, D_2, D_3 at Fig. 3.5) we assumed that the heralded photon was lost. We discarded those cases. We assumed that the lost photons would have behaved the same way as the registered ones (this assumption is commonly called fair sampling).

When we registered a click at a single measurement detector (a heralded click), we assign a value of -1 to the corresponding measurement and $+1$ to the remaining two (see Table 4.1). We can therefore calculate the averages

$$\begin{aligned} \langle A_i A_j \rangle = P(A_i = +1, A_j = +1) &- P(A_i = -1, A_j = +1) \\ +P(A_i = -1, A_j = -1) &- P(A_i = +1, A_j = -1). \end{aligned} \tag{4.5}$$

Because the experiment works with individual heralded photons it is impossible for two measurement detectors to fire simultaneously, i.e. in an ideal experiment we would have:

$$P(A_i = -1, A_j = -1) = 0. \tag{4.6}$$

Nevertheless, in the real world, “accidental” heralded double clicks very occasionally do occur. In our experiment, their contribution was negligible (typically two orders of magnitude smaller than the standard deviation in the rate of heralded single clicks). Therefore, we computed the expectation values using the formula:

$$\begin{aligned}\langle A_i A_j \rangle = P(A_i = +1, A_j = +1) &- P(A_i = -1, A_j = +1) \\ &- P(A_i = +1, A_j = -1).\end{aligned} \tag{4.7}$$

4.2.3 Inaccuracies in the experimental settings

In the first step, the wave plates $WP_1 - WP_4$ are set to $0°$. In the second step, only the orientation of WP_1 is changed and only this wave plate performs a non-trivial transformation. Ideally, the subsequent wave plates should perform no transformation on the polarisation since their orientation is set to $0°$. In reality, this is not the case since their orientation can never be set perfectly. Similar problems occur between stages two and three, and three and four. This is a technical issue rather than a fundamental one, but could be treated similarly to the problem of non-identical measurements. When the wave plates are not set to $0°$, the inaccuracies in orientation are not critical, only affecting the shape of the pentagram and thereby lowering the maximum measurable violation of the inequality. The phase between the two spatial modes should ideally be set to 0. We set the phase with the help of an interference signal of a diode laser. Here, the inaccuracy does not affect our argument. It only decreases the violation that can be observed.

4.3 Classical input to the apparatus

To better understand the physical origin of the violation of the KCBS inequality we check what would happen if we replaced single photons that enter the measurement apparatus with weak coherent states. In this section we will compute the quantum mechanical prediction for this situation for various measurement scenarios.

To simplify the description we consider only the first stage of the hypothetical experiment with classical input, namely the measurement of $\langle A_1 A_2 \rangle$. We depict the corresponding setup at the Fig. 4.2. The classical input is realised by a laser. The laser beam is split by two beam splitters and the outgoing modes are monitored by single-photon detectors. The analysis for the subsequent stages would be analogous. Because of the symmetry of the

KCBS diagram we expect each term of the inequality to give a similar value. This is why we compare the expectation value $\langle A_1 A_2 \rangle$ with one fifth of the non-contextual bound of the KCBS inequality 0.6.

4.3.1 Coherent input state

The coherent state which describes the radiation emitted by a single-mode laser can be expressed in the Fock basis:

$$|\alpha\rangle = e^{-\frac{1}{2}|\alpha|^2} \sum_{n=0}^{\infty} \frac{\alpha^n}{\sqrt{n!}} |n\rangle, \tag{4.8}$$

where $|n\rangle$ represents an n-photon state.

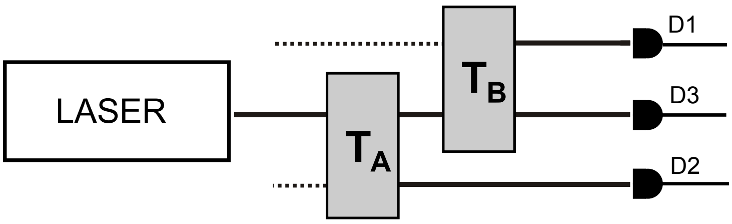

Figure 4.2: The setup that we use to theoretically analyse the predictions for the experiment for the case when the heralded single photon source is replaced by a weak coherent input.

The coherent state splits at the beam-splitters T_A and T_B according to the KCBS geometry. In our experiment the transformations were realised with half-wave plates. Their action can be described by the following matrices (see section 3.4):

$$T_A = \begin{pmatrix} \sin(42°) & 0 & \cos(42°) \\ 0 & 1 & 0 \\ \cos(42°) & 0 & -\sin(42°) \end{pmatrix}, \tag{4.9}$$

$$T_B = \begin{pmatrix} 1 & 0 & 0 \\ 0 & -\sin(26°) & \cos(26°) \\ 0 & \cos(26°) & \sin(26°) \end{pmatrix}. \tag{4.10}$$

For the following analysis only the splitting ratios are relevant. The coefficients c_1, c_2, c_3 correspond to the projections of the input state onto the measurement directions (see Fig. 1.7):

$$c_1 = c_2 = \cos(\widehat{l_1\Psi_0}) = \frac{1}{\sqrt[4]{5}} \approx 0.67, \tag{4.11}$$

$$c_3 = \sqrt{1-2c_1^2} \approx 0.32, \tag{4.12}$$

where $\widehat{l_1\Psi_0}$ denotes the angle between a vector from the KCBS graph l_1 and the vector pointing along the symmetry of the pentagram graph Ψ_0.

We can express the state of the light field before the detectors as a tensor product of coherent states for each mode:

$$|\alpha_T\rangle \equiv |\alpha_1\rangle \otimes |\alpha_2\rangle \otimes |\alpha_3\rangle = |c_1\alpha\rangle \otimes |c_2\alpha\rangle \otimes |c_3\alpha\rangle. \tag{4.13}$$

This is the prepared state that we will consider. We will move on to the description of the measurements.

4.3.2 Measurement – idealised case

Let us start with an idealised description of the measurement. In this case we would not disregard any events. Since the detectors that we use (avalanche photodiodes) do not resolve photon numbers, our measurements can be described by:

$$A_i = 2|0\rangle_i\langle 0|_i - I, \tag{4.14}$$

having ± 1 as eigenvalues. $|0\rangle_i$ denotes a state of 0 photons in mode i. Let us write down the expectation value of the first term of the left-hand side of the KCBS inequality:

$$\langle A_1A_2\rangle_{\alpha_T} = \langle\alpha_T|A_1A_2|\alpha_T\rangle = \langle\alpha_1|A_1|\alpha_1\rangle\langle\alpha_2|A_2|\alpha_2\rangle\langle\alpha_3|\alpha_3\rangle, \tag{4.15}$$

which after using Eqs. 4.14 and 4.8 and inserting the coefficients describing how the coherent input splits (Eqs. 4.11-4.13), yields:

$$\begin{aligned}
\langle A_1A_2\rangle_{\alpha_T} &= \left(2|\langle 0|\alpha_1\rangle|^2 - 1\right)\left(2|\langle 0|\alpha_2\rangle|^2 - 1\right) \\
&= \left(2e^{-|c_1\alpha|^2} - 1\right)\left(2e^{-|c_2\alpha|^2} - 1\right) \qquad (4.16) \\
&= \left(2e^{-\frac{|\alpha|^2}{\sqrt{5}}} - 1\right)^2, \qquad (4.17)
\end{aligned}$$

and clearly $\langle A_1A_2\rangle_{\alpha_T} \geq 0$, so no violation of the classical bound is possible. However if we account for the unequal detection efficiencies we obtain:

$$\langle A_1A_2\rangle_{\alpha_T} = \left(2e^{-\tilde{c}_1\frac{|\alpha|^2}{\sqrt{5}}} - 1\right)\left(2e^{-\tilde{c}_2\frac{|\alpha|^2}{\sqrt{5}}} - 1\right),$$

where the parameters $\tilde{c}_1$ and $\tilde{c}_2$ are the total detection efficiencies (note that, imperfections in the settings of the beam-splitter reflectivities can be inserted into the same coefficients). $\langle A_1A_2\rangle_{\alpha_T}$ becomes negative for certain mean photon numbers as can be seen at the Fig. 4.3. If the differences in detection efficiency are very big, a violation of the classical bound could be observed for certain mean photon numbers. In such situation the same detector would click almost all the time. To violate the classical bound the ratio between the efficiencies would need to be bigger than about 17. In extreme cases (ratio of efficiencies bigger than 42) the registered violation could be stronger than the one predicted by quantum mechanics (see Fig. 4.3). Please note, that this violation is only an indication of a systematic effect and cannot be interpreted as contradicting non-contextual realism or quantum mechanics. The effect can be easily identified – one detector clicking much more often than the others.

4.3.3 Measurement – low detection efficiency

In the real experiment the detection efficiency and losses in the setup prevent us from detecting most of the photons. We do not detect the no-click events directly. Instead we register coincidences between the herald and its "brother-photon" that enters the measurement apparatus. From detecting a coincidence of the heralding detector with e.g. D_1, we learn about the no-click event at D_2 and D_3. We disregard the events when none of the three D_i clicks. This, together with Eq. 4.7 leads us to the following expression

$$\begin{aligned}\langle A_1A_2\rangle &= P(D_3) - P(D_1) - P(D_2)\\ &= 2P(D_3) - 1, \end{aligned} \tag{4.18}$$

where $P(D_i)$ denotes the probability of a click at detector i and was defined in Eq. 4.3.

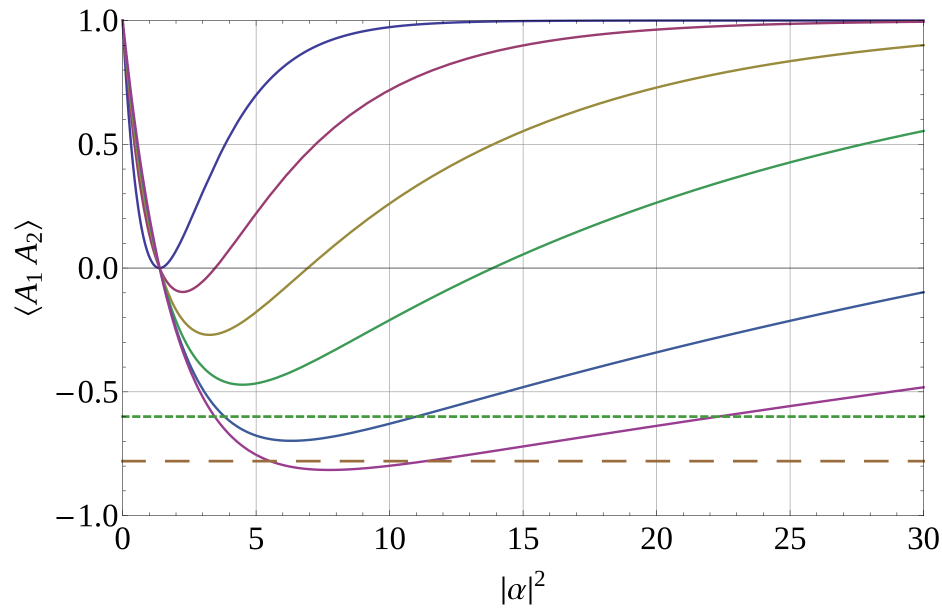

Figure 4.3: Dependence of $\langle A_1 A_2 \rangle_{\alpha_T}$ on the mean photon number of the coherent state $|\alpha|^2$ (solid curves). Different curves correspond to different values of the total detection efficiency of the second detection channel $\tilde{c}_2$: $0.5, 0.2, 0.1, 0.05, 0.02, 0.01$ (starting from the uppermost curve). For all the curves $\tilde{c}_1 = 0.5$. The dotted constant line at -0.6 represents the "classical" bound. The dashed line at -0.78 represents the quantum mechanical prediction for single photons.

In our experiment we used heralded single photons, and this allowed us to identify the cases when the photon was lost. The above formula can be used only for heralded single photons. Without heralding the value assignment that we used would not be justified. In such a case one cannot distinguish the real no-click events from photon loss, therefore one should not disregard the events when none of the measurement detectors clicks. Otherwise one could obtain a violation of the classical bound even with a coherent state input. Moreover the violation would not depend the mean photon number of the coherent state.

A coherent state can approximate a single photon Fock state arbitrarily well if its vacuum component is disregarded. We can verify this by calculating the ratio of probabilities $\frac{p(n>1)}{p(n=1)}$. This ratio can be made arbitrarily small by reducing the mean photon number. Post-selection of non-zero photon number can be easily achieved by only taking into account events when at least one of the detectors clicked.

In summary, if no events are disregarded no violation of the KCBS inequality can be observed under reasonable assumptions. By disregarding the no-click events we open a way for a violation by weak coherent states. Note that, in contrast to the situation with heralded single photons, in the case of weak coherent states there is no physical justification for disregarding the no-click events.

Chapter 5

Conclusions and outlook

5.1 Conclusions

We have presented the first experiment to disprove hidden variable theories (in our case non-contextual) while employing a system that does not allow entanglement. The original proof of the BKS theorem by Kochen and Specker [7] as well as some of the following proofs involved qutrits [23, 22, 57]. The BKS experiments to date, however, have been performed with higher-dimensional systems (mainly pairs of qubits) for which Bell experiments could also be performed [10, 11, 32]. Our experiment involved a single qutrit for which no Bell inequality can be derived.

Our experimental scheme, based on consecutive transformations applied to photon modes and projectors onto path modes, has several advantages. The orthogonality of the modes, which results in the compatibility of the corresponding projectors, makes our experiment immune to the "compatibility loophole" [34].

Moreover the Kochen-Specker value assignment rule (only one of the N projectors onto the basis states can be assigned 1 and the others must be assigned 0) is naturally satisfied in our experiment, because it is not possible for a photon to be found in more than one mode simultaneously.

Each measurement in the KCBS inequality, that we tested in our experiment, appears twice – in two different contexts (accompanied by different measurements commuting with it). When switching between the consecutive terms of the inequality in an experiment one needs to ensure that indeed the same measurement is realised twice. The crucial property of our experiment is that we physically keep the measurements unchanged when changing their context.

Remarkably, our scheme is universal in the sense that it can be applied to any dimension of Hilbert space – one can construct the basis of a Hilbert space from an arbitrary number of paths. The transformations between different projectors can be performed analogously to those in the three-dimensional case.

As the scheme is based on path encoding, it is well suited for realisations with integrated optics, which might be necessary for high-dimensional proofs or situations where high stability is necessary, e.g. for inequalities involving many terms. Integrated optics might also be useful for the entanglement-based and "delayed-choice" scenarios which we discuss below.

5.2 Outlook

State-independence

The original BKS theorem relies on the algebra of observables rathen than on the properties of specific states. However, no state-independent BKS experiment with qutrits has been performed to date. The proofs recently found by Yu and Oh [28] open the way for such experiments [58].

BKS-EPR arguments

Another possible research direction is to combine the ideas of Einstein, Podolsky, and Rosen (EPR) [16] with those of Bell, Kochen, and Specker (BKS) [6, 2, 7]. The use of entangled states allows one to establish the elements of reality based on locality, and then apply the BKS argument to a local subsystem. This idea has been known to the physics community since the early 1980's [59, 60, 57], but there have been no experiments addressing it.

A possible reason for this was the lack of BKS proofs involving the small number of observables and inequalities necessary for experiment feasibility. Experimental schemes and techniques were also missing. Recently, both theoretical and experimental obstacles have been overcome: inequalities have been found [8, 9, 28], and experimental schemes devised [10, 11, 12]. Since 2010, numerous proposals combining EPR and BKS ideas have been published [61, 62, 58].

Our group has recently developed an entangled qubit source which can be easily extended to higher dimensions [63]. This is important since the central part of any EPR-BKS experiment will be an entangled quNit source. In contrast to previous quNit sources, this source is compatible with integrated optics and can generate arbitrary two-quNit states. Our source combined with integrated, tunable multiports forms an ideal platform for EPR-BKS experiments in higher dimensions.

Delayed choice of the measurement settings

Another possible extension is motivated by a peculiar feature of our experiment: the choice between the two measurements that accompany a given measurement could be made after this measurement is performed, e.g. the choice between A_1 and A_3 could be made after A_2 was measured. Note that this can only be done between the measurements which are connected by a single transformation, in other words, the loose-ends problem would not allow this idea to be applied to all the pairs of measurements.

In a follow-up experiment, the measurement settings could be chosen after the photons have left the preparation stage, which might be relevant to the argument devised by Bub and Stairs [64].

Theoretical implications

Interestingly, the EPR-BKS argument requires only the perfect correlations, whereas the Bell theorem involves statistical predictions of quantum mechanics. This makes the EPR-BKS argument similar to the the Greenberger-Horne-Zeilinger version of the Bell theorem [65]. In the EPR-BKS, however, already locally there is a conflict between quantum mechanics and non-contextual realism. It is elevated to a conflict with local realism by the presence of entanglement [61]. In some situations, perfect correlations can be derived from basic physical principles (e.g. the conservation of angular momentum). This suggests that the EPR-BKS experiment will have different implications than a Bell experiment. The connection to the conservation laws suggests that the physical implementation of the observables might affect the conclusions of the experiment. Some of the theoretical implications of the EPR-BKS argument have already been analysed [66, 67, 68], but the physical realisation was not taken into account. Note that an EPR-BKS experiment can be viewed as an experimental realisation of the scenario analysed by Conway and Kochen in the context of the "Free-will theorem" [57].

Bibliography

[1] B. Carpenter, "The Prose Poetry of Zbigniew Herbert: Forging a New Genre," *The Slavic and East European Journal*, vol. 28, pp. 76–88, Apr. 1984.

[2] J. S. Bell, "On the problem of hidden variables in quantum mechanics," *Reviews of Modern Physics*, vol. 38, pp. 447–452, July 1966.

[3] S. J. Freedman and J. F. Clauser, "Experimental test of local hidden-variable theories," *Phys. Rev. Lett.*, vol. 28, pp. 938–941, April 1972.

[4] A. Aspect, J. Dalibard, and G. Roger, "Experimental test of Bell's inequalities using time- varying analyzers," *Physical Review Letters*, vol. 49, pp. 1804–1807, Dec. 1982.

[5] G. Weihs, T. Jennewein, C. Simon, H. Weinfurter, and A. Zeilinger, "Violation of Bell's inequality under strict Einstein locality conditions," *Physical Review Letters*, vol. 81, pp. 5039–5043, Dec. 1998.

[6] E. Specker, "Die Logik nicht gleichzeitig entscheidbarer Aussagen," *Dialectica*, vol. 14, pp. 239–246, Sept. 1960.

[7] S. Kochen and E. Specker, "The problem of hidden variables in quantum mechanics," *Journal of Mathematics and Mechanics*, vol. 17, no. 1, 1967.

[8] A. A. Klyachko, M. A. Can, S. Binicioğlu, and A. S. Shumovsky, "Simple test for hidden variables in spin-1 systems," *Phys. Rev. Lett.*, vol. 101, p. 020403, July 2008.

[9] A. Cabello, S. Filipp, H. Rauch, and Y. Hasegawa, "Proposed experiment for testing quantum contextuality with neutrons," *Physical review letters*, vol. 100, no. 13, p. 130404, 2008.

[10] G. Kirchmair, F. Zahringer, R. Gerritsma, M. Kleinmann, O. Guhne, A. Cabello, R. Blatt, and C. F. Roos, "State-independent experimental test of quantum contextuality," *Nature*, vol. 460, pp. 494–497, July 2009.

[11] E. Amselem, M. Radmark, M. Bourennane, and A. Cabello, “State-Independent quantum contextuality with single photons,” *Physical Review Letters*, vol. 103, p. 160405, Oct. 2009.

[12] R. Lapkiewicz, P. Li, C. Schaeff, N. K. Langford, S. Ramelow, M. Wiesniak, and A. Zeilinger, “Experimental non-classicality of an indivisible quantum system,” *Nature*, vol. 474, pp. 490–493, June 2011.

[13] W. H. Wollaston, “A method of examining refractive and dispersive powers, by prismatic reflection,” *Philosophical Transactions of the Royal Society of London*, vol. 92, pp. 365–380, Jan. 1802.

[14] E. C. Watson, “Reproductions of Prints, Drawings, and Paintings of Interest in the History of Physics. 48. William Hyde Wollaston and the Discovery of the Dark Lines in the Solar Spectrum,” *American Journal of Physics*, vol. 20, no. 8, pp. 496–498, 1952.

[15] J. Fraunhofer, “Bestimmung des Brechungs- und des Farbenzerstreungs-Vermoegens verschiedener Glasarten, in Bezug auf die Vervollkommnung achromatischer Fernroehre,” *Annalen der Physik*, vol. 56, pp. 264–313, Jan. 1817.

[16] A. Einstein, B. Podolsky, and N. Rosen, “Can Quantum-Mechanical description of physical reality be considered complete?,” *Physical Review*, vol. 47, pp. 777–780, May 1935.

[17] J. F. Clauser, M. A. Horne, A. Shimony, and R. A. Holt, “Proposed experiment to test local Hidden-Variable theories,” *Physical Review Letters*, vol. 23, pp. 880–884, Oct. 1969.

[18] N. D. Mermin, “Hidden variables and the two theorems of John Bell,” *Rev. Mod. Phys.*, vol. 65, pp. 803–815, July 1993.

[19] J. V. Neumann, *Mathematical foundations of quantum mechanics*, vol. 2. Princeton Univ Pr, 1996.

[20] A. Einstein, *Albert Einstein, philosopher-scientist*, vol. 7. Library of Living Philosophers, 1949.

[21] D. Bohm, “A Suggested Interpretation of the Quantum Theory in Terms of "Hidden" Variables. I,” *Phys. Rev.*, vol. 85, pp. 166–179, Jan 1952.

[22] A. Peres, *Quantum theory: concepts and methods*, vol. 57. Kluwer Academic Publishers, 1993.

[23] A. Peres, “Two simple proofs of the Kochen-Specker theorem,” *Journal of Physics A: Mathematical and General*, vol. 24, no. 4, p. L175, 1991.

[24] M. Kernaghan, “Bell-Kochen-Specker theorem for 20 vectors,” *Journal of Physics A: Mathematical and General*, vol. 27, p. L829, 1994.

[25] M. Kernaghan and A. Peres, “Kochen-Specker theorem for eight-dimensional space,” *Physics Letters A*, vol. 198, no. 1, pp. 1 – 5, 1995.

[26] A. Cabello, J. Estebaranz, and G. Garcia-Alcaine, “Bell-Kochen-Specker theorem: A proof with 18 vectors,” *Physics Letters A*, vol. 212, pp. 183 – 187, 1996.

[27] M. Pavicic, J. Merlet, B. McKay, and N. D. Megill, “Kochen-Specker vectors,” *Journal of Physics A: Mathematical and General*, vol. 38, pp. 1577–1592, Feb. 2005.

[28] S. Yu and C. H. Oh, “State-Independent proof of Kochen-Specker theorem with 13 rays,” *Physical Review Letters*, vol. 108, p. 030402, Jan. 2012.

[29] N. D. Mermin, “Simple unified form for the major no-hidden-variables theorems,” *Physical Review Letters*, vol. 65, p. 3373, Dec. 1990.

[30] C. Simon, M. Zukowski, H. Weinfurter, and A. Zeilinger, “Feasible ’Kochen-Specker’ experiment with single particles,” *Physical Review Letters*, vol. 85, no. 9, pp. 1783 – 1786, 2000.

[31] Y. Huang, C. Li, Y. Zhang, J. Pan, and G. Guo, “Experimental test of the Kochen-Specker theorem with single photons,” *Physical Review Letters*, vol. 90, p. 250401, June 2003.

[32] H. Bartosik, J. Klepp, C. Schmitzer, S. Sponar, A. Cabello, H. Rauch, and Y. Hasegawa, “Experimental test of quantum contextuality in neutron interferometry,” *Physical Review Letters*, vol. 103, p. 040403, July 2009.

[33] P. Badziag, I. Bengtsson, A. Cabello, and I. Pitowsky, “Universality of state-independent violation of correlation inequalities for noncontextual theories,” *Physical review letters*, vol. 103, no. 5, p. 50401, 2009.

[34] O. Guehne, M. Kleinmann, A. Cabello, J.-A. Larsson, G. Kirchmair, F. Zaehringer, R. Gerritsma, and C. F. Roos, “Compatibility and noncontextuality for sequential measurements,” *Physical Review A*, vol. 81, p. 022121, Feb. 2010.

[35] R. W. Spekkens, "Contextuality for preparations, transformations, and unsharp measurements," *Physical Review A*, vol. 71, p. 052108, May 2005.

[36] R. W. Spekkens, "Negativity and contextuality are equivalent notions of nonclassicality," *Physical Review Letters*, vol. 101, p. 020401, July 2008.

[37] R. W. Spekkens, D. H. Buzacott, A. J. Keehn, B. Toner, and G. J. Pryde, "Preparation contextuality powers Parity-Oblivious multiplexing," *Physical Review Letters*, vol. 102, p. 010401, Jan. 2009.

[38] P. Badziag, I. Bengtsson, A. Cabello, H. Granstrom, and J.-A. Larsson, "Pentagrams and paradoxes," *Foundations of Physics*, vol. 41, pp. 414–423, Mar. 2010.

[39] A. A. Klyachko, M. A. Can, S. Binicioğlu, and A. S. Shumovsky *unpublished, private communication*, Oct. 2009.

[40] A. Cabello *private communication*, Nov. 2009.

[41] M. Wiesniak *private communication, unpublished*, Apr. 2009.

[42] D. A. Meyer, "Finite precision measurement nullifies the Kochen-Specker theorem," *Physical Review Letters*, vol. 83, pp. 3751–3754, Nov. 1999.

[43] N. D. Mermin, "A Kochen-Specker theorem for imprecisely specified measurement," *quant-ph/9912081*, Dec. 1999.

[44] C. Simon, a. Brukner, and A. Zeilinger, "Hidden-Variable theorems for real experiments," *Physical Review Letters*, vol. 86, pp. 4427–4430, May 2001.

[45] D. M. Appleby, "Nullification of the nullification," *arXiv:quant-ph/0109034*, Sept. 2001.

[46] J. Larsson, "A Kochen-Specker inequality," *EPL (Europhysics Letters)*, vol. 58, p. 799, 2002.

[47] A. Cabello, "Finite-precision measurement does not nullify the Kochen-Specker theorem," *Physical Review A*, vol. 65, no. 5, p. 052101, 2002.

[48] D. Appleby, "The Bell-Kochen-Specker theorem," *Studies In History and Philosophy of Science Part B: Studies In History and Philosophy of Modern Physics*, vol. 36, pp. 1–28, Mar. 2005.

[49] A. Kent, "Noncontextual hidden variables and physical measurements," *Physical Review Letters*, vol. 83, pp. 3755–3757, Nov. 1999.

[50] R. Clifton and A. Kent, "Simulating quantum mechanics by Non-Contextual hidden variables," *Proceedings of the Royal Society of London. Series A: Mathematical, Physical and Engineering Sciences*, vol. 456, pp. 2101–2114, Sept. 2000.

[51] H. Havlicek, G. Krenn, J. Summhammer, and K. Svozil, "Colouring the rational quantum sphere and the Kochen-Specker theorem," *Journal of Physics A: Mathematical and General*, vol. 34, pp. 3071–3077, Apr. 2001.

[52] J. Barrett and A. Kent, "Non-contextuality, finite precision measurement and the Kochen-Specker theorem," *Studies In History and Philosophy of Science Part B: Studies In History and Philosophy of Modern Physics*, vol. 35, no. 2, p. 151â176, 2004.

[53] M. Reck, A. Zeilinger, H. J. Bernstein, and P. Bertani, "Experimental realization of any discrete unitary operator," *Physical Review Letters*, vol. 73, pp. 58–61, July 1994.

[54] M. Zukowski, A. Zeilinger, and M. Horne, "Realizable higher-dimensional two-particle entanglements via multiport beam splitters," *Physical Review A*, vol. 55, no. 4, p. 2564, 1997.

[55] A. Zeilinger, "General properties of lossless beam splitters in interferometry," *American Journal of Physics*, vol. 49, no. 9, p. 882, 1981.

[56] J. Sakurai and S. Tuan, *Modern quantum mechanics.* Addison-Wesley Pub. Co.(Reading, Mass.), 1994.

[57] J. Conway and S. Kochen, "The free will theorem," *Foundations of Physics*, vol. 36, pp. 1441–1473, Oct. 2006.

[58] A. Cabello, E. Amselem, K. Blanchfield, M. Bourennane, and I. Bengtsson, "Proposed experiments of qutrit state-independent contextuality and two-qutrit contextuality-based nonlocality," *Phys. Rev. A*, vol. 85, p. 032108, Mar 2012.

[59] P. Heywood and M. Redhead, "Nonlocality and the Kochen-Specker paradox," *Foundations of Physics*, vol. 13, pp. 481–499, May 1983.

[60] A. Stairs, "Quantum logic, realism, and value definiteness," *Philosophy of Science*, vol. 50, pp. 578–602, Dec. 1983.

[61] A. Cabello, “Proposal for revealing quantum nonlocality via local contextuality,” *Physical Review Letters*, vol. 104, p. 220401, June 2010.

[62] A. Cabello and M. T. Cunha, “Proposal of a Two-Qutrit contextuality test free of the finite precision and compatibility loopholes,” *Physical Review Letters*, vol. 106, p. 190401, May 2011.

[63] C. Schaeff, R. Polster, R. Lapkiewicz, R. Fickler, S. Ramelow, and A. Zeilinger, “Scalable fiber integrated source for higher-dimensional path-entangled photonic quNits,” *Optics Express*, vol. 20, 2012.

[64] J. Bub and A. Stairs, “Contextuality and nonlocality in ’no - signaling’ theories,” *0903.1462*, Mar. 2009.

[65] D. M. Greenberger, M. A. Horne, A. Shimony, and A. Zeilinger, “Bell’s theorem without inequalities,” *American Journal of Physics*, vol. 58, no. 12, pp. 1131–1143, 1990.

[66] H. Brown and G. Svetlichny, “Nonlocality and Gleason’s lemma. Part 1. Deterministic theories,” *Foundations of Physics*, vol. 20, pp. 1379–1387, Nov. 1990.

[67] A. Elby, “Nonlocality and Gleason’s lemma. Part 2. Stochastic theories,” *Foundations of Physics*, vol. 20, pp. 1389–1397, Nov. 1990.

[68] A. Elby, “On the physical interpretation of Heywood and Redhead’s algebraic impossibility theorem,” *Foundations of Physics Letters*, vol. 3, pp. 239–247, June 1990.

Acknowledgements

My first thanks go to my supervisor Anton Zeilinger for the great research and study opportunities he gave to me, for his inspiring questions, for teaching me to dare in physics, to question what the theoreticians say, and for his openness to new ideas (even the crazy ones).

I would like to thank all the people I worked with (also those who I do not mention here) for the fantastic atmosphere and all the things I learned from them. Christoph, for your cool experimental ideas, hints in the lab, for giving the insider tour of Texas, for the appreciation of the "most basic sport", and for all the EMALI trips. Robert, for your toughness in fighting all the (experimental) difficulties, for sharing your philosophy and experimental insights, and for the fantastic Käsespätzle! Sven, for your support in all kinds of situations when I was confused – both in physics and in the rest of the world. Robert, for your amazing electronics skills and for accompanying me when I was alone in Vienna. Mario, the Murau ambassador, for your enthusiasm for physics (night discussions about Zilches), for your special attitude to Austria and Murau, and for talking Austrian to me! Sascha, for your solid, critical approach to designing the experiments and for our lab discussions. Peizhe, for being a great team-mate in the lab. When I arrived in Vienna in 2008, I shared my office with Stefano, Borivoje and Matteo. Big thanks to you for making every working day fun!

Thanks also to Dany, Verena, Manuela, Ursula, Andrea, Aylin and the administration from the University for their help during my years in Vienna.

I am very grateful to the "editorial team." The editor in chief: Marissa, and the editors: Bill, Christoph, Robert and Robert helped me a lot to improve the language and the clarity of the thesis. Thank you for your great work! Still, I don't give up authorship of all the errors.

I thank my Mom and Dad for their constant support and real interest in what I do, even when it is a single photon experiment testing an inequality based on the Bell-Kochen-Specker theorem. Finally, the biggest thanks to Maja, Ula and Janek for their support, without which I wouldn't make it to this stage.

Finally I would like to thank the funding institutions. We were generously supported by the European Research Council (Advanced Grant QIT4QAD), the Austrian Science Fund (Grant F4007), the European Commission (Marie Curie Research Training Network EMALI), and the Vienna Doctoral Program on Complex Quantum Systems (CoQuS).

Curriculum Vitae

PERSONAL INFORMATION

Name:	Radosław Łapkiewicz
Date of birth:	26/01/1984
Place of birth:	Toruń, Poland

EDUCATION

08/2010	Secondment, University of California, Berkeley
10/2008 – present	PhD studies, University of Vienna
03/2007 – 06/2007	Erasmus Scholarship, University of Vienna
2003 – 2008	Studies of Physics, University of Warsaw
1999 – 2003	The Forth Public High School, Toruń

GRANTS AND HONORS

01/2009 – 09/2010	Marie Curie Fellowship – *Engineering, Manipulation and Characterization of Quantum States of Matter and Light*
09/2007	Research Scholarship – *Bilateral collaboration between universities of Vienna and Warsaw*
2002	Finalist of the Polish National Physics Olympiad
1998 – 2003	Polish Children's Fund Scholarship

PUBLICATIONS

1. *Experimental non-classicality of an indivisible quantum system*
R. Lapkiewicz, P. Li, C. Schaeff, N. K. Langford, S. Ramelow, M. Wiesniak, A. Zeilinger
Nature, 23. June 2011 | DOI: 10.1038/nature10119

2. *Scalable fiber integrated source for higher-dimensional path-entangled photonic quNits*
C. Schaeff, R. Polster, R. Lapkiewicz, R. Fickler, S. Ramelow, A. Zeilinger
Optics Express, vol. 20, 2012

3. *Entanglement of Photons with Adjustable Singularities*
M. Krenn, R. Fickler, M. Huber, R. Lapkiewicz, W. N. Plick, S. Ramelow, A. Zeilinger
submitted; preprint: quant-ph/1205.2514

4. *Entanglement of Very High Quanta of Angular Momentum*
R. Fickler, R. Lapkiewicz, W. N. Plick, M. Krenn, C. Schaeff, S. Ramelow, A. Zeilinger
submitted; preprint: quant-ph/1207.2376